8-2009

CHARACTERIZATION AND ENHANCEMENT OF SENSING PROPERTIES OF PIEZOELECTRIC MATERIALS WITH APPLICATIONS TO VIBRATION SUPPRESSION

Siddharth Aphale
Clemson University, saphale@clemson.edu

CHARACTERIZATION AND ENHANCEMENT OF SENSING PROPERTIES OF PIEZOELECTRIC MATERIALS WITH APPLICATIONS TO VIBRATION SUPPRESSION

A Thesis Presented to the

Graduate School of Clemson University

In Partial Fulfillment

of the Requirements for the Degree

Master of Science

Mechanical Engineering

by

Siddharth Aphale

August 2009

Accepted by:

Dr. Nader Jalili, Committee Chair

Dr. Darren M. Dawson

Dr. Gang Li

Abstract

This thesis undertakes the study of piezoelectric properties of polymer-based fabric and film sensors. An enhancement in piezoelectric properties of such sensors, as noted through earlier work, is observed with increasing weight ratios of nanomaterials dispersed in the polymer matrix. A comprehensive mathematical model using cantilever beams is developed to analyze this enhancement both qualitatively and quantitatively. An experimental setup is also developed to implement the proposed real time signal processing necessary to collect required data towards the characterization. In order to distinguish piezoelectric materials from other materials, study of the frequency response of developed fabric sensors to periodic chirp type actuation signals, is also established.

Linear Euler-Bernoulli beam theory is used, to model piezoelectric actuation of cantilever beams. The theory has been extended to integrate piezoelectric sensing with the governing equations of motion to obtain a numerical solution to the governing partial differential equation of motion. All equations are derived using a distributed-parameters model applying the extended Hamilton Principle. Results obtained are compared to base values from literature for known materials.

Piezoelectric materials are also known to possess bi-stiffness properties, having a higher modulus of elasticity in their open circuit configuration as compared to that in their short circuit configuration. Through research, it has been observed that the weight ratio of dispersed nanomaterials does not affect the piezoelectric properties alone but also has an effect on the mechanical properties and beyond a threshold, established for every polymer analyzed, the increase in the tensile properties of the fabric developed cannot be ignored. This study is extended to analyze the enhancement in the difference between the two moduli of elasticity for the fabric sensors in their respective configurations. The bi-stiffness elements can be used effectively to suppress vibrations implementing a semi-active vibration damping method known as ‘Switched Stiffness’. This concept

is studied in regard to continuous systems, and the underlying principle of switching between two configurations is mathematically modeled. The developed control law for vibration suppression is then integrated using non-contact type measurement of tip deflection to suppress vibrations induced in cantilever beams, using the fabric sensors developed at Clemson University. The damping characteristics have been analyzed to study the enhancement in the difference between the higher and lower stiffness values and qualitative conclusions are drawn.

Using the mathematical modeling developed to implement the 'Switched Stiffness' concept, a novel method to measure the coupling coefficient, k_{31}, a characteristic constant for piezoelectric materials, is established and validated. The results of this measurement are used to decouple the piezoelectric properties from the mechanical properties and a generalized framework to completely characterize piezoelectric materials towards other constants has been proposed.

DEDICATION

To my family and my friend Parikshit Mehta

ACKNOWLEDGEMENTS

I am thankful to my faculty advisor, Dr. Nader Jalili for his continue guidance and support during this phase of my education. I am indebted to my fellow student and friend Parikshit Mehta for his continued support both as a friend and a fellow researcher. I also want to thank my advisory committee, Dr. Darren Dawson and Dr. Gang Li for their important suggestions and academic inputs. Continuous support from Dr. Mohammed Daqaq in the area of perturbation methods is also appreciated.

TABLE OF CONTENS

LIST OF FIGURES

LIST OF TABLES

Chapter 1

Introduction

1.1 Research Background and Literature Review

The pyroelectric effect, characterized by the generation of electric field in response to temperature gradient across a material, was studied by Carolus Linnaeus and Franz Aepinus in the mid-18th century. Working on this base, both René Just Haüy and Antoine César Becquerel put forth a theory relating the mechanical stress and electric charge [1]. Their formulations, however, were never established experimentally.

The direct piezoelectric effect, which similar to the pyroelectric effect is observed in crystals with no defined plane of symmetry, is characterized by the generation of an electric potential in response to a mechanical strain induced in the material. It was first demonstrated in 1880 by the brothers Pierre Curie and Jacques Curie. "Developing on the knowledge of pyroelectricity, they integrated their understanding of the underlying crystal structures to predict crystal behaviour. The direct piezoelectric effect was first demonstrated in the crystals of tourmaline, quartz, topaz, cane sugar and Rochelle salt (sodium potassium tartrate tetrahydrate)" [1].

This early work establishing that mechanical strain can generate equivalent electric potential in certain materials, which were established as those whose crystals have no defined plane of symmetry, led to extensive work in identifying such materials and trying to develop a technology that could exploit this phenomenon. Through such studies; polymers like PVDF, PAN, Nylon and Polyurea were studied and characterized to be piezoelectric materials.

"The 20th century witnessed a revolution in the area of material science and fabrication of new materials with certain properties facilitating some of the revolutionary technologies developed over the major war periods. One major phase of this revolution was the scientific approach to development and characterization of nanomaterials. For quite a few centuries, nanotechnology was being used without the realization of its true potential in processes like the manufacturing of steel and vulcanization of rubber. The first scientific observations and size measurements were however initiated in the first decade of the 20th century, often associated with Richard Adolf Zsigmondy. Richard made a detailed study of gold sols and a range of other nanomaterials with sizes as small as 10 nm or even less. He used ultramicroscope, employing the dark field method for observing particles with sizes much less than light wavelength. Zsigmondy was also the first one to use the nanometer explicitly for characterizing particle size. He determined it as 1/1,000,000 of millimeter. The next significant discovery in the area of nanomaterials highly significant to the area of piezoelectricity was that of carbon nanotubes" [2].

"In 2006, an editorial published in the journal Carbon, by Marc Monthioux and Vladimir Kuznetsov established the one of the earliest recorded research related to discovery of carbon nanotubes, which being hollow tubes of nanometer range diameters composed of graphite carbon. This discovery is often wrongly associated with Sumio Iijima of NEC, in 1991" [2].

Further research which evolved around nanomaterials, nanotubes and their production validated that nanomaterials too are highly piezoelectric. However with the health and functionality related issues with such materials as singled wall nanotubes, it was difficult to exploit these properties to build a new technology. Nanomaterials have been long classified as highly carcinogenic materials.

This limitation changed the course of thought and a novel idea of dispersing the nanomaterials in a polymer matrix to enhance the original piezoelectric properties of the piezo-polymers emerged. For

implementing this idea effectively, two major processes in effect for a long time for other purposes were selected; Electrospinning and Spin Coating [3,4].

The rapid development in technologies like infusion pumps, power electronics and power amplifiers enabled the setup of a novel experimental bench to automate these processes and stimulate the research in fabric sensors and actuators which have the potential of revolutionalizing the field of NEMS and MEMS as well as areas like energy harvesting and vibration suppression. Developing on the setup of electrospinning engineered at Clemson University in 2002-03 [5], the piezoelectric effect of a variety of polymers like PVDF, PAN, Polyurea and Nylon has been explored. Expanding the project from the manufacturing of piezoelectric fabric sensors and actuators and the static analysis of the piezoelectric effect, the Euler Bernoulli beam theory is used to develop a dynamic analysis. The initial analysis work was setup under the laser vibrometer of the MSA 400.

The NSF leased MSA 400 system is used to analyze the mode shapes and perform frequency domain analysis on the nonlinearities of NEMS and MEMS. Based on these experiments at micro/nano scale, a macro level experiment has been developed to analyze the vibrations produced in the fabric sensors through base excited motion and measure the corresponding voltage produced. The base excited motion of the sensors has been modeled as base excitation to an Euler Bernoulli beam and then the piezoelectric effect was modeled using the constitutive equations of piezoelectricity [6].

1.2 Research Motivation

As discussed above, the direct piezoelectric effect is characterized by the generation of a proportional electric potential across a piezoelectric material when subjected to mechanical strain. Thus, if one is able to induce strain in a controlled manner across a piezoelectric material, the electric potential developed can be extracted and used to harvest energy. This makes such materials a huge potential as

renewable sources of energy as long as the strain does not exceed the permanent charge saturation limit. Recently, there has been significant research in the extraction of energy from mechanically strained structures using piezoelectric materials. For example, the tires of automobile are under continuous mechanical strain and stress when rolling along the road. The variation in friction between the ground and the tires further enhances this strain. If a piezoelectric sensor was to be embedded into the tire surface, the strain induced in the tire could be extracted as useful energy through the sensor. Another fascinating example of energy harvesting from piezoelectric materials is in the case of vibrating structures. Structures such as the blades of a turbine are continuously under lateral stress and strain. This strain energy can be harvested in addition to the energy harvested from wind or flowing fluid and thus the effective process efficiency can be enhanced.

The energy harvesting application as seen clearly requires a process where vibrations are either imminent or desired. On the other hand, in most applications, vibrations are undesirable. For example the vibrations in the members of towers or construction work are undesired. Vibrations in moving machinery detiorate the life span of moving elements. In such areas, these vibrations need to be suppressed. Piezoelectric materials as established through research are bi-stiffness materials. These materials have potentionally different mechanical stiffness. If the two ends of a piezoelectric sensor are shorted, the effective mechanical stiffness reduces than the mechanical stiffness possessed in the open circuit configuration. Using this peculiar characteristic, an effective semi-active vibration scheme, commonly known as ‘switched stiffness’ [7, 8], has been developed to suppress undesirable vibrations.

The converse piezoelectric effect renders these materials as good actuators as well as good candidate for active vibration control schemes by applying a control voltage designed to induce out-of-phase vibrations in the vibrating member using the piezo-actuator. This application however has the

limitation of real time frequency domain analysis to measure the vibrations in the member and then apply voltage corresponding to the out-of-phase vibrations which cancel off the net effect. Another limitation of this active vibration control scheme is that for a causal system there is a finite delay involved in the computation of the control signal and therefore the cancellation may not be effective. This limitation has been overcome to some extent by integrating a feedforward term computed through numerical pre-processing of the equations but, this process is tedious in general. The amplitude of voltage signal required to suppress the vibrations is another limitation. For all these reasons, the semi-active vibration suppression schemes are preferred.

Through this work an attempt to analyze all these aspects of piezoelectric materials and come up with one integrated platform to characterize these materials completely has been made. Another aspect of the research is the extension of the semi-active scheme to being an active vibration suppression method. Modeling the effective damping enhancement related to the switch stiffness control law, based on an equivalent structural damping model, am attempt to design a active vibration control signal from this effective damping model has been made, which has overcome most of the above limitations. This being our motivation we will now discuss the thesis contributions.

1.3 Thesis Contributions

A detailed process description and optimization of process conditions has been presented for the process of Electrospinning applied to an automated fabrication unit for manufacturing of piezoelectric fabric sensors. The effect of concentration of nanotubes dispersed in a polymer matrix in comparison to the polymer concentration has been studied for PVDF, PAN and Nylon. This effect has been then correlated to the enhancement in sensing properties of the piezo-sensors. The effect of infusion rate, voltage applied and distance between the capacitor plates in electrospinning on the quality of sensors has been studies in detail. Working on a macro level experiment based on the

principle of vibration analysis of cantilever beams, a non-contact type displacement measurement integrated test bench has been developed. Through detailed frequency and time domain analysis, the vibrations induced in the cantilever beam via various techniques have been correlated to the piezoelectric effect observed in the fabric sensors. Both qualitative and quantitative comparisons of enhancement in piezoelectric properties as a function of the weight ratio of the nanomaterials dispersed in the polymer matrix have been graphed. The electromechanical coupling effect has been studied with the integration of the back EMF effect in case of free vibrations and the frequency shift has been modeled to analyze the enhancement better. Developing on this work, the switch stiffness scheme has been implemented to demonstrate vibration suppression in continuous systems and to establish the bi-stiffness property of piezoelectric materials. A novel velocity observer has been used to implement the switch stiffness control law and a software based switching logic has been designed for actual experimentation. The experiment has been modeled mathematically to characterize the piezoelectric materials completely. Finally, an equivalent viscous damping model has been developed to model the discontinuous control law and thus integrating this model in to the EOM, a novel active vibration control scheme has been designed and implemented. In addition, FEM has been applied to solve the free and forced, linear and nonlinear vibrations of Euler-Bernoulli beam and a feedforward term has been added to get better control efficiency for vibration suppression. The FEM solution has also been used to correlate the enhancement in the piezoelectric constants numerically.

1.4 Thesis Layout

This thesis discusses the experimental validation and analysis of the characterization of piezoelectric polymer sensors, along with the enhancement in the piezoelectric properties by controlled dispersion of nanomaterials in the polymer matrix. This, the first chapter, gives the introduction to the research, clarifying the intent and the direction of work. It also outlines the stages of contribution and the

various aspects of the work. The second chapter focuses on the process of electrospinning as applied to a fabrication unit for piezoelectric polymer sensors and the initial analysis. This chapter begins with the detailed layout and working principle of the actual process. Following this, the optimization of the process conditions is discussed with the related lookup table drawn in detail. An overview of previously existing automation is then followed by the initial static and dynamic testing and the establishment of a base to distinguish piezoelectric materials from the other materials. The experimental bench setup under the MSA 400 leased by NSF is then explained in detail followed by the results of this work.

The third chapter begins with the need to setup a macro stage cantilever beam experiment separately with a non-contact laser sensing integration. The cantilever beam experiment is then modeled based on the Euler-Bernoulli beam theory [9], stating all the assumptions explicitly. The stress-strain relationship is then established without any assumptions and the energy method is used to apply the extended Hamilton's principle [9] to obtain the mathematical model. The corresponding boundary conditions are then analyzed and the separation of variables is discussed in detail. The results of the experiment are then discussed and tabulated with appropriate inferences explained at the end of the chapter. The next chapter discusses the separation of variables at length as a way to solve the EOM and analyze the vibrations. Limitations of this method are clarified and a general finite element model is developed for a generalized solution. The solution to both free and forced vibrations is then analyzed in both time and frequency domain. This analysis leads the need of analysis of nonlinear vibrations and the EOM for the modified Euler-Bernoulli beam theory for large vibrations is derived again using the extended Hamilton's Principle. The solution to this EOM is then attempted by separation of variables, clarifying the failure and thus the importance of FEM in the area of vibration control. The results using this new model are then discussed with updates on the accuracy improvement.

The fifth chapter introduces the concept of switch stiffness as a semi-active vibration control scheme in detail. The mathematical modeling is presented in detail with emphasis on the novel velocity observer designed for the real time implementation of the vibration suppression scheme. The primarily designed observer is then modified based on a detailed Lyapunov analysis to yield better results. This is followed by the stability analysis of both the observer and the integrated nonlinear system with both the observer and controller. The discussion is then extended to characterizing the piezoelectric materials better and the results of this section are then presented along with a detailed interpretation. Chapter 6 is an extension of the theoretical work of chapter 5 to the actual experimental bench. The bi-stiffness property of the piezoelectric materials is discussed in detail and the experimental implementation to continuous systems is discussed. The discussion is then extended to benefits of active vibration control scheme over a semi-active one and based on this an effective viscous damping model for the switch stiffness control law is proposed and validated. Following up, a novel active vibration control scheme has been developed which overcomes the limitations of delays detiorating real time implementation of other active vibration control schemes and the limitation on amplitude of the voltage signal. The results are then tabulated in detail and appropriate inferences are explained.

In chapter 7, the complete work is summarized and the characterization is compiled in one single result section, presenting an integrated novel test bench to completely characterize any piezoelectric material. This is our contribution through this research carried over the last two years. The scope of work in the future is then drawn at the conclusion.

Chapter 2

PROCESS DESCRIPTION: ELECTROSPINNING

2.1 Electrospinning

'In the 16th century, William Gilbert was studying the behaviour of magnetic and electrostatic phenomena, when he observed that when a significantly electrically charged particle of amber was brought in the vicinity of water, it would change the surface into a cone from the tip of which small droplets of water would eject. Based on this, the first observation of electrospraying, J.F. Cooley developed and patented the process now popularly known as electrospinning in 1902' [3]. The process of electrospinning can be better explained by referring to Figure 2.1.

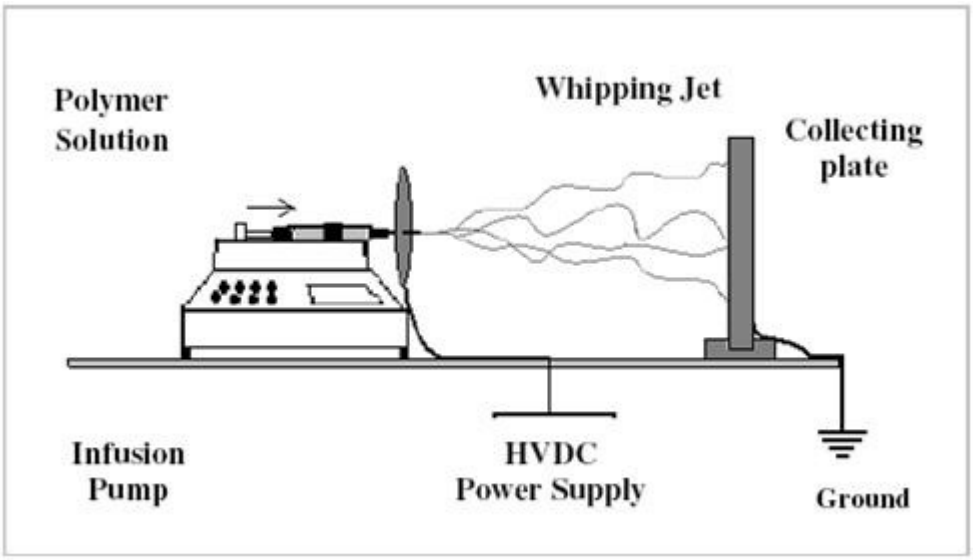

Figure 2.1 The process of electrospinning [5].

The process consists of an infusion syringe pump which hosts a syringe containing the solution to be electrospun. The positive plate of a parallel plate capacitor rests from the needle of this syringe. The negative plate of this capacitor arrangement is used as the collector. When a significant voltage difference is applied across the plates, liquid droplets infused into the developed field by the pump

form a Tyndall's cone [3, 5] from the tip of which the droplets get stretched into thin fibres whose diameter can be controlled adjusting the process parameters, i.e. infusion rate, voltage difference and the distance between the parallel plates.

"A nonaxisymmetric model is considered for the analysis of the jet whose centerline is curved. As the jet bends, the surface charge density is no more uniform across the cross section of the jet. Hence, the potential equations for this model have to be modified to account for the higher order nonaxisymmetric distortions. Under real conditions, the centerline is curved due to the domination of whipping instabilities and hence all the force, torque and electric field equations are based on this model. There are different modes in which the electrospinning process takes place. These include; (i) dripping, (ii) spindle or spray mode, and (iii) whipping jet mode. The equation of motion due to effect of both electrical field and surface charge can be given by equation" [5]:

$$\rho\pi h^2\ddot{x}(s)=\left(\pi h\gamma+\frac{h^2{E_\infty}^2(\beta+2)}{4}\right)\frac{1}{R}- \left(\frac{h^2{E_\infty}^2\bar{\varepsilon}(\beta+2)}{4\pi}\frac{\bar{\varepsilon}}{K}\right)\frac{\partial}{\partial t}\frac{1}{R}-\left(\frac{3}{4}\pi h^4\mu+\frac{\bar{\varepsilon}}{32\pi}\frac{h^4{E_\infty}^2\bar{\varepsilon}}{K}\right)\frac{\partial}{\partial t}\frac{\partial^2}{\partial s^2}\left(\frac{1}{R}\right) \tag{2.1}$$

This EOM is derived based on the momentum balance, i.e. Navier Stokes equations [5]. It is observed that when charge density increases to more than the surface tension, the instabilities in the jet arise. Hence, equation of motion has to be modified to include additional terms due to surface charge. Although such generalization will involve both linear and nonlinear stages of the whipping phenomenon, in most practical cases $h \ll R$ and $h \ll L$ (where L is the contour length of the jet), and hence, higher order derivatives of s involving h/R and h/L can be safely neglected. This simplifies the equation of motion to the following final form,

$$\rho\pi h^2\ddot{x}(s)=2\pi h\sigma_0 E_\infty\hat{\xi}+\left(\pi\gamma+\frac{h(E_\infty\hat{t})^2\beta\bar{\varepsilon}}{2}+\frac{2h\pi^2{\sigma_0}^2}{\bar{\varepsilon}}(3-2\ln\chi)\right)\frac{h}{R} \tag{2.2}$$

Here, $\chi = R/h$ is the dimensionless wavelength of instability [5].

2.2 Optimization of process conditions

As a part of this research, the most optimum set of conditions under which a polymeric solution in a suitable solvent with varied weight ratios of nano-particles can produce the best quality fabric through the process of Electrospinning has been established. In this process, a polymeric solution, made by sonicating the polymer in a suitable solvent, is injected using an infusion pump in the region of a high electric field applied through application of very high voltage through 2 parallel plate conductors. In the field created by the voltage, the infused solution spins on the surface of a Tindal's Cone [3, 5] and finally fibers are drawn by the withdrawal of solvent under the spin effect. These fibers form an unwoven fabric at the collector, which can be also designed such as to weave through the fibers produced.

Based on extensive experimental work, three major parameters that influence the fiber diameter which is the eventual measure of process quality have been identified. These parameters are; voltage applied at the parallel plates, the infusion rate at the infusion pump and the distance between the two conductor plates [5]. The exact nature of the influence of these parameters on the fiber diameter has not been put into mathematical equations but work is being put into quantifying these relations for designing an adaptive controller for better quality. The relations established through empirical formulations are highly non-linear but the approximate relations are:

- Fiber diameter reduces as the distance between the conductor plates increases.
- Fiber diameter increases with increase in the infusion rate
- Fiber diameter reduces as the voltage applied increases.

Not only are the exact relations non-linear but also they are interactive in nature and not independent. So through running of numerous experiments under varying set of conditions, the most optimum

conditions for each type of solution have been established. These conditions are reported in Table 2.1.

Table 2.1 Optimized process condition sets for various polymer and nanomaterial combinations.

Type of Solution	**Optimum Voltage (kV)**	**Optimum Infusion Rate (ml/min)**	**Optimum distance (cm)**
Pure PVDF	24-32	0.05-0.15	10-15
PVDF with SWNTs	28-34	0.02-0.08	10-15
PVDF with ZnO	24-30	0.05-0.12	10-15
Pure PAN	22-30	0.05-0.3	10-20
PAN with SWNTs	24-30	0.05-0.2	10-15
PAN with ZnO	24-30	0.05-0.3	10-15
PAN with C60	24-30	0.05-0.4	10-15

Following the determination of these critical sets, fabrics of varying thickness and varying dimensions were produced successfully and tested initially under static modes. The results of static measurements of the piezo constants showed that with the doping of the polymer solution with nano-particles the piezo properties improved. However to establish this fact and for measuring the exact enhancement, dynamic measurements were necessary.

An experimental bench consisting of a fixed-free cantilever beam was designed for the necessary dynamic measurements. Using the fabric produced with the process as an actuator, a cantilever beam was excited through a chirp signal. Studying the signal processing applied to the measured data; the natural frequencies of the beam were recorded through the displacement and velocity measurements by means of the laser vibrometer. Then, the beam was base excited with the same chirp signal and the fabric patch was used as a sensor and the voltage produced was measured. Mathematically modeling these two experiments using Euler-Bernoulli beam theory [9], mathematical tools like MATLAB have been used to computationally solve the equations of motion and thereby solve for the piezoelectric constant, d_{31}. The computed values were then compared with the literature and they have matched within 10% error. This established a means to make the measurements dynamic. Using the same concept of laser vibrometer, a novel dynamic measurement system has been established for both the fabric as well as the film sensors. The results of the experiments carried out have been compared with literature data and the cross verification has been successful. Displayed in Figure 2.2 are the pictures of the newly designed experimental setup at Clemson University.

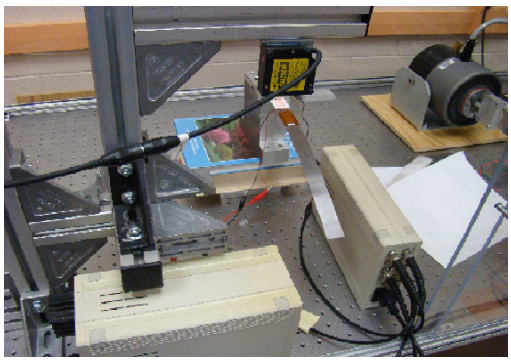

(A)

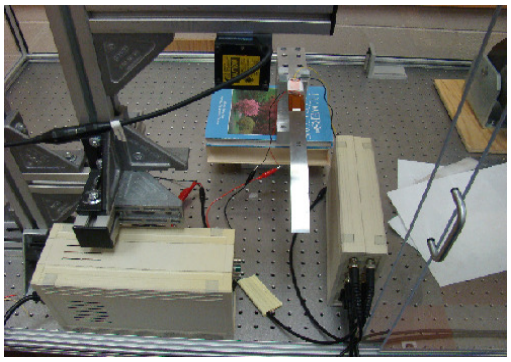

(B)

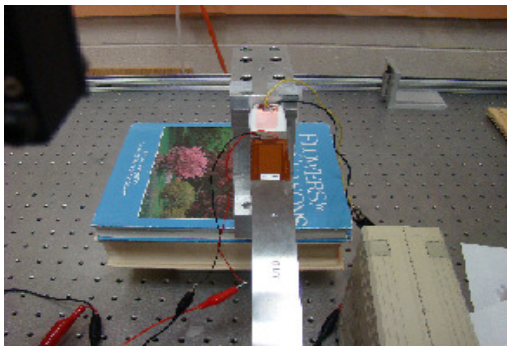

(C)

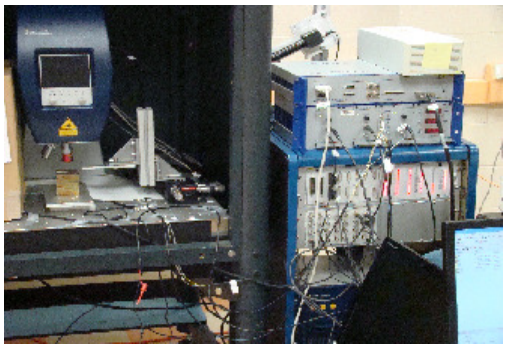

(D)

Figure 2.2 (A) and (B) The new experimental setup, (C) Close up of the cantilever beam with the commercial actuator and fabric sensor, (D) The set up with the DSPACE board for MSA 400

The plots in Figure 2.3 graph the results obtained for the dynamic response of the beam at '$x = L$'. It can be seen clearly that as the concentration of SWNTs increases, the corresponding average amplitude of the output transverse displacement increases significantly. This is reinstated through the last plot comparing the three results. This supports the increase in the value of 'd_{31}' as the concentration of SWNTs increases. The observed increase in sensor response for 0.05% SWNTs is 9.5X.

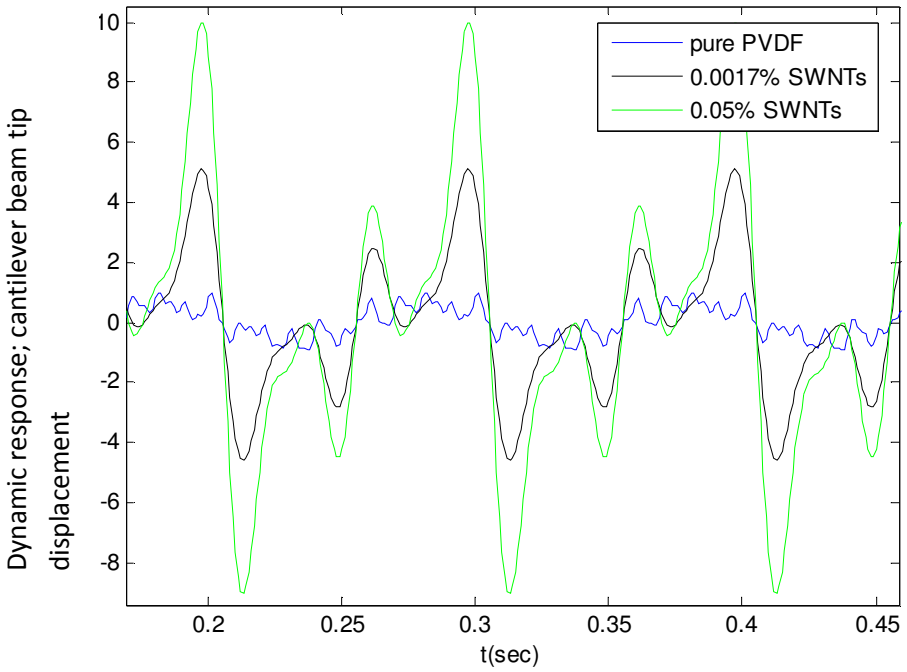

Figure 2.3 The **Normalized** dynamic response of the piezo fabric sensor observed under the MSA 400

The MSA 400 is the microsystem analyzer leased to Clemson University by NSF. These measurements have shown the enhancement in the piezo properties of the polymer fabric. The enhancement in the 0.0017% weight ratio sample has been measured to be 1.5-2 times and that in the 0.05% weight ratio is 8-10 times. This initial measurement through the actuator model has been refined and backed up from the sensor approach. The experimental setup has been show in the pictures above. The results of the final computational model are discussed in the Section 2.3.1.

2.3 Discussion of Results

2.3.1 RESULTS: Piezoelectric properties of PVDF

Table 2.2 Tabulated Results for PAN (Fabric)

Type of Nano-particles	Weight Ratios(%)/Enhancement in sensor response (X times)			
SWNTs	0.01/1.2	0.02/2.8	0.05/6	
ZnO	0.02/2.2			
C60	0.02/1.6			

Table 2.3 Tabulated Results for PAN (Film)

Type of Nano-particles	Weight Ratios(%)/Enhancement in sensor response (X times)
SWNTs	0.02/2.5
ZnO	0.02/2.3
C60	0.02/1.5

Table 2.4 Tabulated Results for PVDF (Fabric)

Type of Nano-particles	Weight Ratios(%)/Enhancement in sensor response (X times)			
SWNTs	0.01/2.5	0.02/5	0.05/9.5	0.1/16.5
ZnO	0.02/4.2			

Table 2.5 Tabulated Results for PVDF (Film)

Type of Nano-particles	Weight Ratios(%)/Enhancement in sensor response (X times)
SWNTs	0.02/4.7 0.05/8.2
ZnO	0.02/3.8
C60	0.02/4.6

Now, these results have been obtained under estimated parameter model of the Young's Modulus of Elasticity and the Moment of Inertia, '*I*' for the sample under test. This is because samples are not available enough to undertake destructive testing of the fabric or the films to measure these parameters and average them out over the range for one type of sample. Hence we have estimated these values in the above data set scaling up the base values on the available literature. Expanding this range intellectually to broaden the spectrum and lessen the error, we have taken a range of these parameter values in the range of plus-minus 250 units. The results for the computation on this range are tabulate in the Section 2.3.2.

2.3.2 RESULTS: Piezoelectric properties of PAN

Table 2.6 Tabulated Results for PAN (Fabric)

Type of Nano-particles	Weight Ratios(%)/Enhancement in sensor response (X times)
SWNTs	0.01/1-1.6 0.02/2.2-3.4 0.05/3.2-7.8
ZnO	0.02/1.5-2.6
C60	0.02/1-2.8

Table 2.7 Tabulated Results for PAN (Film)

Type of Nano-particles	Weight Ratios(%)/Enhancement in sensor response (X times)
SWNTs	0.02/2-3.1
ZnO	0.02/1.7-3.2
C60	0.02/1.3-2.6

Table 2.8 Tabulated Results for PVDF (Fabric)

Type of Nano-particles	Weight Ratios(%)/Enhancement in sensor response (X times)
SWNTs	0.01/1.8-3.4 0.02/3.6-5.8 0.05/6.2-10.3 0.1/12-17.8
ZnO	0.02/3.5-5

Table 2.9 Tabulated Results for PVDF (Film)

Type of Nano-particles	Weight Ratios(%)/Enhancement in sensor response (X times)
SWNTs	0.02/3.6-6 0.05/7.5-9.8
ZnO	0.02/3.1-4.2
C60	0.02/3.4-7.2

The three basic parameters that are of interest to us from the point of view of characterization are: the piezo-electric constant d_{31}, the tensile modulus of elasticity and the damping characteristics. To get a qualitative comparison in enhancement of the vibration dampening characteristics, we need to simply monitor the impulse response of the beam with the patch firmly attached to the beam. Extensive experiments have been carried out towards this characterization and the results are tabulated below. Here the calculation of the damping ratio is based on the logarithmic decay ratio model. **Please note**

that the interpretation of these values is necessarily qualitative at this stage and enhancement is noted comparatively.

Table 2.10 Comparative study of the damping characteristics w.r.t. the weight ratio of dispersed nanomaterials.

Serial No.	Weight Ratio of SWNTs (%)	Damping Ratio
1	Pure PVDF	$2.42*10^{-3}$
2	0.02	$5.36*10^{-3}$
3	0.05	$15.25*10^{-3}$
4	0.1	$39.76*10^{-3}$
5	0.2	$124.77*10^{-3}$
6	0.25	$231.68*10^{-3}$

From these sets of results it can be seen that there is an effect of variation in the weight ratio of dispersed nanomaterials on the piezoelectric properties of the polymer fabric sensors. However, a similar enhancement in the actuation properties is yet to be established, as polymer fabric sensors are not good actuators for these properties to be detected by the available equipment.

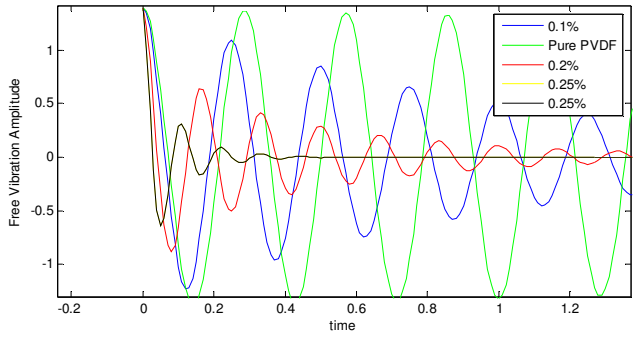

Figure 2.4 Curve fitted plots of the response of the free end of the macro beam, under the influence of damping properties of piezoelectric sensor attached.

Chapter 3

MATHEMATICAL MODELING: VIBRATIONS OF CANTILEVER BEAMS

3.1 System Description and Assumptions:

To establishing a fundamental mathematical model for the experimental bench designed, a model based on cantilever beams with the PZT actuator bonded on its top surface and the sensor attached at the bottom has been considered [6]. The beam has a uniform cross-section with thickness t_b and length l, and the PZT actuator has a uniform thickness t_p and length (l_2-l_1). The PZT actuator is bonded perfectly to the beam at distance of l_1 from the fixed end. We assume that the voltage applied to the actuator is only an external signal and independent of x. This assumption is valid for length of the PZT being very small compared to the length of the beam which is valid under Euler-Bernoulli beam theory assumptions [9].

3.1.1 Mathematical Modeling:

For convenience of all, a uniform coordinate system is defined, the x-axis being along the longitudinal direction and the z-axis specified in the transverse direction with the mid-plane of the beam corresponding to $z=0$. This coordinate system is fixed at the base of the beam. This is shown in the Figure 3.1 [6].

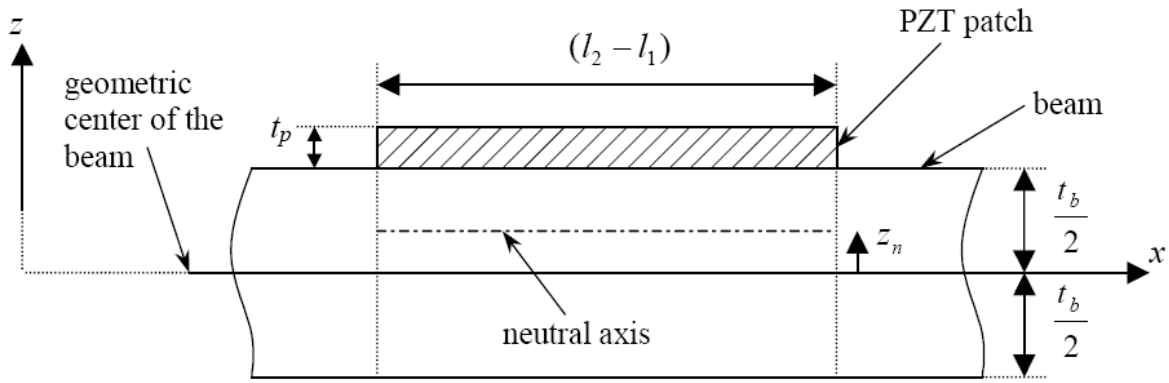

Figure 3.1 Nomenclature w.r.t. PZT patch bonded to the beam [6].

It is assumed in this discussion that there is no axial deformation of the beam and small deflection assumption holds. The resultant displacement field under these assumptions is represented by [9]:

$$u = -z\frac{\partial w(x,t)}{\partial x}, v = 0, w = w(x,t) \tag{3.1}$$

where u, v, w are the beam displacements in the x-, y-, z- directions respectively. w denotes the transverse displacement of the mid-plane of the beam. Utilizing this displacement field, it is trivial that the only non-zero strain component for the beam is given by:

$$\varepsilon_{xx} = \frac{\partial u}{\partial x} = \frac{\partial(-z\frac{\partial w(x,t)}{\partial x})}{\partial x} = -z\frac{\partial^2 w(x,t)}{\partial x^2} \tag{3.2}$$

Equation 3.2 is valid if and only if z is measured from the neutral axis of the flexible member. Since the PZT actuator is not along the entire length of the beam, the neutral axis shifts in the region where the PZT is bonded to the beam. To extend this discussion into determining the strain induced in the PZT, we need to first relocate the neutral axis. It is given by [6]:

$$\int_{-\frac{t_b}{2}}^{\frac{t_b}{2}} E^b\left(z-z_n\right)dz+\int_{\frac{t_b}{2}}^{\frac{t_b}{2}+t_p} E^p\left(z-z_n\right)dz=0 \tag{3.3}$$

On simplifying, we get

$$z_n = E^b t_p(t_p+t_b)/2(E^b t_b + E^p t_p) \tag{3.4}$$

where, E^b and E^p are the Young's modulus of elasticity of the beam and PZT respectively.

Hence, the non-zeros strain in the beam is given by:

$$\varepsilon_{xx} = \begin{Bmatrix} -z\dfrac{\partial^2 w(x,t)}{\partial x^2}, x < l_1 and x > l_2 \\ -(z-z_n)\dfrac{\partial^2 w(x,t)}{\partial x^2}, l_1 < x < l_2 \end{Bmatrix} \tag{3.5}$$

The stress in the beam is related to the strain using Hooke's Law [9],

$$\sigma_{xx} = E^b \varepsilon_{xx} \tag{3.6}$$

3.1.2 Modeling the PZT:

The piezoelectric effect was discovered by Pierre and Jacques Curie in 1880 [1]. The direct piezoelectric effect consists of the ability of certain crystalline materials (polymers in our interest) to generate an electrical charge in proportion of an externally applied force. The direct effect is used in force transducers. According to the inverse piezoelectric effect, an electric field parallel to the direction of polarization induces an expansion of material. The piezoelectric effect is anisotropic [1]. It can only be exhibited by materials whose crystal structure has no center of symmetry.

The direction of expansion with respect to the direction of the electrical field depends on the constants appearing in the constitutive equations. The material can be manufactured in such a way that one of the coefficients dominates the others. Piezoelectric actuators are becoming increasingly important in micro-positioning technology.

The fundamental relations for piezoelectric materials are given by;

$$\mathbf{S} = \mathbf{s}^{\mathbf{E}}\mathbf{T} + \mathbf{d}\mathbf{E}^{\mathbf{p}} \tag{3.7}$$

$$\mathbf{D} = \mathbf{d}\mathbf{T} + \varepsilon^{\mathbf{T}}\mathbf{E}^{\mathbf{p}} \tag{3.8}$$

These are the fundamental constitutive equations of piezoelectricity [6]. These equations are in general matrix representations. We however do not use this generalized form since in piezoelectric materials with specific application to structural vibration control, one direction dominates the others. Using these relationships, we can now formulate the strain in the PZT.

Since we are using the laminar design of the PZT actuator, the *z-x* (31) interaction is dominant and the strain induced in the PZT is given by:

$$\sigma_{xx} = E^p \varepsilon_{xx} - E^p d_{31} v(t) / t_p \tag{3.9}$$

where *v(t)* is the excitation voltage applied across the actuator.

3.1.3 Derivation of Equations of Motion (Extended Hamilton's principle):

The strain energy of the system (π) can be expressed as:

$$\pi = \frac{1}{2}(\sigma_{xx}\varepsilon_{xx} + \sigma_{yy}\varepsilon_{yy} + \sigma_{zz}\varepsilon_{zz} + \tau_{xy}\gamma_{xy} + \tau_{xz}\gamma_{xz} + \tau_{zy}\gamma_{zy})dV \tag{3.10}$$

$$\pi = \frac{b}{2}\int\int(\sigma_{xx}\varepsilon_{xx})dA \tag{3.11}$$

$$\pi = \frac{b}{2}\left[\begin{array}{l}\int_0^{l_1}\int_{-\frac{t_b}{2}}^{\frac{t_b}{2}} E^b\left(\frac{\partial^2 w(x,t)}{\partial x^2}\right)^2 z^2 dzdx + \int_{l_1}^{l_2}\int_{-\frac{t_b}{2}}^{\frac{t_b}{2}} E^b\left(\frac{\partial^2 w(x,t)}{\partial x^2}\right)^2 (z-z_n)^2 dzdx \\ +\int_{l_1}^{l_2}\int_{\frac{t_b}{2}}^{\frac{t_b}{2}+t_p} E^p\left(\frac{\partial^2 w(x,t)}{\partial x^2}\right)^2 (z-z_n)^2 dzdx + \int_{l_1}^{l_2}\int_{\frac{t_b}{2}}^{\frac{t_b}{2}+t_p} E^p d_{31}\frac{v(t)}{t_p}\frac{\partial^2 w(x,t)}{\partial x^2}(z-z_n)dzdx + \\ \int_{l_2}^{l}\int_{-\frac{t_b}{2}}^{\frac{t_b}{2}} E^b\left(\frac{\partial^2 w(x,t)}{\partial x^2}\right)^2 z^2 dzdx\end{array}\right] \tag{3.12}$$

$$\pi = \frac{b}{2}\left[\begin{array}{l}\left\{\int_0^{l} E^b(\frac{\partial^2 w(x,t)}{\partial x^2})^2 \frac{{t_b}^3}{12}dx\right\} + \left\{\int_{l_1}^{l_2} E^b\left(\frac{\partial^2 w(x,t)}{\partial x^2}\right)^2 ({t_b}{z_n}^2)dx\right\} \\ +\left\{\int_{l_1}^{l_2} E^p\left(\frac{\partial^2 w(x,t)}{\partial x^2}\right)^2 (\frac{1}{3}{t_p}^3 + \left(t_p\left(\frac{t_b}{2}\right)^2 + \left(\frac{t_b}{2}\right)(t_p)^2\right) - z_n\left((t_p)^2 + t_p t_b\right) + t_p {z_n}^2)dx\right\} \\ +\left\{\int_{l_1}^{l_2} 0.5E^p d_{31}\frac{v(t)}{t_p}\left(\frac{\partial^2 w(x,t)}{\partial x^2}\right)((t_p)^2 + (t_p t_b) - 2t_p z_n)dx\right\}\end{array}\right] \tag{3.13}$$

The strain energy can be now expressed in short hand as,

$$\pi = \frac{1}{2}\int_0^{l} EI(x)(\frac{\partial^2 w(x,t)}{\partial x^2})^2 dx + \frac{b}{2}\int_0^{l} 0.5E^p d_{31} v(t)(t_p + t_b - 2z_n)s(x)\left(\frac{\partial^2 w(x,t)}{\partial x^2}\right)dx \tag{3.14}$$

The kinetic energy of the system (T) is given by:

$$T = \frac{1}{2}\int_0^{l}\rho A(x)(\frac{\partial w(x,t)}{\partial t})^2 dx \tag{3.15}$$

There is no external work as a function of input applied since the applied external voltage has been incorporated in the strain energy using the constitutive equations of piezoelectricity, but we need to consider the effect of gravity, in case of the practical experimental setup.

$$W = \int_0^l \rho A(x)\, g w(x,t) dx \tag{3.16}$$

Applying extended Hamilton's principle [9], we have:

$$\int_{t_1}^{t_2} \delta(T - \pi + W)\, dt = 0 \tag{3.17}$$

Now, we have

$$\delta\int_{t_1}^{t_2} \pi dt = \int_{t_1}^{t_2}\int_0^l EI(x)\left(\frac{\partial^2 w(x,t)}{\partial x^2}\right)\left(\frac{\partial^2 \delta w(x,t)}{\partial x^2}\right) dx dt$$
$$+\frac{b}{2}\int_{t_1}^{t_2}\int_0^l 0.5 E^p d_{31} v(t)\left(t_p + t_b - 2z_n\right) s(x)\left(\frac{\partial^2 \delta w(x,t)}{\partial x^2}\right) dx dt \tag{3.18}$$

$$\delta\int_{t_1}^{t_2} \pi dt = \int_{t_1}^{t_2}\{\left[EI(x)\left(\frac{\partial^2 w(x,t)}{\partial x^2}\right)\frac{\partial \delta w(x,t)}{\partial x}\right]_0^l - \left[\frac{\partial}{\partial x}(EI(x)\left(\frac{\partial^2 w(x,t)}{\partial x^2}\right))\delta w(x,t)\right]_0^l$$
$$+\int_0^l \frac{\partial^2 (EI(x)\left(\frac{\partial^2 w(x,t)}{\partial x^2}\right))}{\partial x^2}\delta w(x,t)\, dx\} dt$$
$$+\frac{b}{2}\int_{t_1}^{t_2}\int_0^l 0.5 E^p d_{31} v(t)\left(t_p + t_b - 2z_n\right)\left(\frac{\partial^2 s(x)}{\partial x^2}\right)\delta w(x,t)\, dx dt \tag{3.19}$$

Similarly,

$$\delta\int_{t_1}^{t_2} T dt = \int_{t_1}^{t_2}\int_0^l \rho A(x)\frac{\partial^2 w(x,t)}{\partial t^2}\delta w(x,t)\, dx dt \tag{3.20}$$

The resulting EOM is given by:

$$\rho A(x)_n \frac{\partial^2 w(x,t)}{\partial t^2} + \frac{\partial^2}{\partial x^2}\left(EI(x)_n \frac{\partial^2 w(x,t)}{\partial x^2} \right) = \frac{\partial^2}{\partial x^2}\left(-0.5bE^p d_{31} v(t)\left(t_p + t_b - 2z_n\right) s(x)\right) + \rho A(x)_n g \tag{3.21}$$

with fixed-free boundary conditions.

Note that in this derivation, all the terms in the integral have been retained since the effect of all the terms is significant for the exact dimensions of the system under consideration. Also, the effect of gravity can be ignored by deriving these equations from the equilibrium point.

Now let us discuss the solution to this EOM. The EOM derived in (3.21) can be expressed as,

$$\rho A(x) \frac{\partial^2 w(x,t)}{\partial t^2} + \frac{\partial^2}{\partial x^2}\left(EI(x) \frac{\partial^2 w(x,t)}{\partial x^2} \right) = f(x,t) \tag{3.22}$$

Assuming that a solution to this non-linear partial differential equation exists and that the *x*-coordinate is separable from the temporal coordinate, let us assume the solution to be in the form of an assumed mode expansion.

$$w(x,t) = \sum_i W_i(x) q_i(t) \tag{3.23}$$

where, $W_i(x)$ is the spatial mode shape and $q_i(t)$ are the temporal coordinates. Substituting this close form solution in the boundary conditions, we can solve for the spatial mode shapes as,

$$W_i(x) = \cos\cos(\beta_i x) - \cosh(\beta_i x) - \left(\frac{\cos\cos(\beta_i l) + \cosh(\beta_i l)}{\sin\sin(\beta_i l) + \sinh(\beta_i l)} \right)(\sin\sin(\beta_i x) - \sinh(\beta_i x)) \tag{3.24}$$

where $\beta_i l \cong (2i-1)(\frac{\pi}{2})$

If we substitute the assumed mode expansion of the solution in the equation of motion, we have:

$$\sum_i (\rho A(x) W_i(x) \ddot{q}_i + \frac{\partial^2}{\partial x^2}\left(EI(x) W_i^{"}(x)\right) q_i = f(x,t) \tag{3.25}$$

Multiplying both sides of the equation by $W_j(x)$ and integrating over the domain, we can use the orthogonality condition of the modes to reform the equations. Thus we have:

$$\ddot{q}_i + \omega_i^2 q_i = \int_0^l W_i(x) f(x,t) dx \tag{3.26}$$

The experimental bench is shown in Figure 3.2.

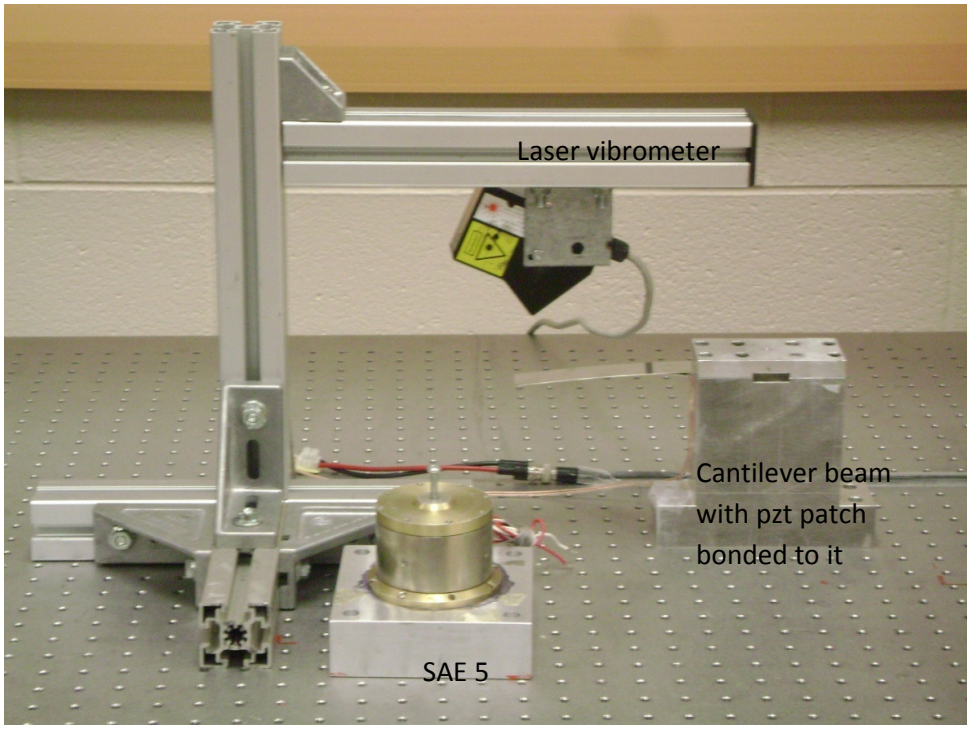

Figure 3.2 Experimental setup.

3.2 Modeling the Sensor:

Using the constitutive equations of piezoelectricity, we can express the charge developed on the sensor as a function of the vibrations induced in the beam by:

$$Q = 0.5bE^s d_{31s}\left(l_2 - l_1\right)\left(\frac{\partial w\left(l_2,t\right)}{\partial x} - \frac{\partial w\left(l_1,t\right)}{\partial x}\right) \tag{3.27}$$

where, E^s is the Young's modulus of electricity of the sensor material and d_{31s} is the piezoelectric constant of the sensor [6]. In this equation we assume the thickness of the sensor and the actuator to be the same.

Now using the linear model of a parallel plate capacitor which is the structure of the sensor, we have:

$$v\left(t\right) = Q / C_p \tag{3.28}$$

where, C_p is the capacitance of the sensor which can be measured using an impedance measurement circuit. Thus by measuring the voltage output at the sensor electrodes and feed-forwarding the solution of the EOM, we can solve for the term ($E^s d_{31s}$). The results of this characterization are tabulated in Tables 3.1 to 3.5.

Table 3.1 Results of characterization of sensors based on matrix of PVDF and SWNTs.

Serial No.	**Weight Ratio of SWNTs (%)**	$E^s d_{31f}$ (Averaged over 10 readings)
1	Pure PVDF $E^s = 1.103*10^9$(Pa)	0.0254 Theoretical 0.0267 Experimental
2	0.02	0.0837
3	0.05	0.1547
4	0.1	0.2109
5	0.2	0.4326
6	0.25	0.5821

Table 3.2 Results of characterization of sensors based on matrix of PVDF and C60.

Serial No.	**Weight Ratio of C60 (%)**	$E^s d_{31f}$ (Averaged over 10 readings)
1	Pure PVDF $E^s = 1.103*10^9$(Pa)	0.0254 Theoretical 0.0267 Experimental
2	0.05	0.1752
3	0.1	0.2357
4	0.25	0.5264

Table 3.3 Results of characterization of sensors based on matrix of PVDF and ZnO.

Serial No.	**Weight Ratio of C60 (%)**	$E^s d_{31f}$ (Averaged over 10 readings)
1	Pure PVDF $E^s = 1.103*10^9$(Pa)	0.0254 Theoretical 0.0267 Experimental
2	0.05	0.1352
3	0.1	0.1964
4	0.25	0.5372

Table 3.4 Results of characterization of sensors based on matrix of PAN and SWNTs.

Serial No.	**Weight Ratio of SWNTs (%)**	$E^s d_{31f}$ (Averaged over 10 readings)
1	Pure PAN $E^s = 0.5667*10^9$(Pa)	0.0017 Theoretical 0.0012 Experimental
2	0.05	0.0091
3	0.1	0.0137
4	0.25	0.0312

Table 3.5 Results of characterization of sensors based on matrix of PAN and C60.

Serial No.	**Weight Ratio of SWNTs (%)**	$E^s d_{31f}$ (Averaged over 10 readings)
1	Pure PAN $E^s = 0.5667*10^9$(Pa)	0.0017 Theoretical 0.0012 Experimental
2	0.05	0.0103
3	0.1	0.0183

3.3 Interpretation:

The results tabulated above show clearly that the dispersion of nanomaterials in the polymer matrix enhances the piezoelectric properties of these polymers significantly. However, note that it is the product $E^s d_{31f}$ that gets enhanced, i.e. the addition of nanomaterials to polymer matrix enhances the electromechanical properties and not just the electrical. This observation leads to the conclusion that there exists an electromechanical coupling. Thus, the mechanical strain and electrical effect is coupled and hence it can be expected that a back EMF effect is observed when analyzing the data closely. This is a topic of the chapters to come but still a point worth the mention here. It is this electromechanical coupling that makes the system highly nonlinear and note that empirical constitutive equations have been used to establish this coupling, in which the effect of higher order terms may be ignored. Let us now explore this in more detail in the chapters to come.

Chapter 4

SOLUTION TO GOVERNING EQUATION: AN EXPANSION TO MODELING NONLINEAR VIBRATIONS OF CANTILEVER BEAMS

4.1 Introduction and Literature Review:

In the previous chapter, the linear vibrations of a cantilever beam have been analyzed based on the linear Euler-Bernoulli beam theory [9]. Both piezoelectric actuation as well as sensing involved in the base experiment to characterize the piezoelectric materials have been modeled based upon the constitutive equations of piezoelectricity [6]. Now, to mathematically characterize these materials, a solution to the governing equation needs to formulated based on which the measurement data needs to be post processed, integrating the solution into a set of integral equations. This chapter introduces the two most widely used methods of obtaining the solution to the partial nonlinear multivariable differential equation at hand; Assumed Mode analysis and Finite Element Analysis (FEA) [9, 24]. To explain the method of finite elements and its necessity as a tool to obtain the solution, it is useful to discuss the tool of Finite Difference Method (FDM) [24], not a part of this work, and its limitations that leads to the analysis using FEA.

The governing equations derived in the previous chapter were based on the assumption of small vibration amplitude which inherently implies linear strain. However, the experimental conditions are not limited to these assumptions and the experimental bench at the macro level requires analysis taking into consideration large vibration amplitude i.e. nonlinear strain. The results using the linear strain theory and their divergence from expected accuracy is discussed after the section on solution to the governing equations derived in the previous chapter. This discussion is then expanded to the derivation of the more accurate governing equations based on nonlinear strain theory. Following this extensive mathematical modeling the failure of modal analysis is then elaborated extending the discussion to the only feasible method of solution, FEA. The finite element formulation is then

addressed in detail finally compiling the results. In the final section, the characterization of piezoelectric materials based on this analysis is revisited and the improvement is established through comparison. In the appendix A1, all the relevant numerical analysis files are attached herewith.

4.2 Modal analysis and assumed mode expansion theory:

As discussed in brief in the previous chapter, one method to obtain a numerical solution to the governing equation of vibrations of a cantilever beam based on the Euler-Bernoulli beam theory (linear strain) is the method of assumed mode analysis. The solution is assumed to be separable in space and time, i.e. it is assumed that there is no coupling within the solutions on the two separate variables. Thus the solution can be written as,

$$w(x,t) = W(x)\phi(t) \tag{4.1}$$

The fixed-free boundary conditions associated with the vibrations of a cantilever beam are given by,

$$\begin{aligned} &w(0,t) = 0, \frac{\partial w}{\partial x}(0,t) = 0 \\ &\frac{\partial^2 w}{\partial x^2}(l,t) = 0, \frac{\partial^3 w}{\partial x^3}(l,t) = 0 \end{aligned} \tag{4.2}$$

The homogeneous governing equation of vibration of a beam based on the linear Euler-Bernoulli beam theory is given by,

$$\rho A(x)\frac{\partial^2 w(x,t)}{\partial t^2} + \frac{\partial^2}{\partial x^2}\left(EI(x)\frac{\partial^2 w(x,t)}{\partial x^2} \right) = 0 \tag{4.3}$$

For a beam with uniform cross-section, this reduces to

$$\rho A\frac{\partial^2 w(x,t)}{\partial t^2} + EI\left(\frac{\partial^4 w(x,t)}{\partial x^4} \right) = 0 \tag{4.4}$$

Substituting the assumed separable form of solution in this homogeneous governing equation, we have

$$\rho A W(x)\frac{d^2\phi(t)}{dt^2}+EI\left(\frac{\partial^4 W(x)}{\partial x^4}\right)\phi(t)=0 \tag{4.5}$$

i.e.

$$\frac{\dfrac{d^2\phi(t)}{dt^2}}{\phi(t)}+\frac{EI}{\rho A}\frac{\left(\dfrac{\partial^4 W(x)}{\partial x^4}\right)}{W(x)}=0 \tag{4.6}$$

Thus, both the ratios in the above equation have to be of opposite signs. The ratio, $\dfrac{\dfrac{d^2\phi(t)}{dt^2}}{\phi(t)}$ cannot be positive since the solution would not be oscillatory which we know is harmonic. For the solution to be harmonic,

$$\frac{\dfrac{d^2\phi(t)}{dt^2}}{\phi(t)}=-\omega^2 \tag{4.7}$$

Thus, we have

$$\frac{\left(\dfrac{\partial^4 W(x)}{\partial x^4}\right)}{W(x)}=\frac{\omega^2}{c^2}=\beta^4 \text{ where, } c=\sqrt{\frac{EI}{\rho A}} \tag{4.8}$$

i.e.

$$\left(\frac{\partial^4 W(x)}{\partial x^4}\right)-\beta^4 W(x)=0 \tag{4.9}$$

Let us assume the solution to the above governing equation of the spatial mode to be exponential, i.e.

$W(x) = Ce^{sx}$ where C and s are constants. Substituting this assumption into the governing equation, we have

$s^4 - \beta^4 = 0$, the roots of which are $s = \pm\beta$ and $s = \pm i\beta$

Thus the spatial solution can be written compactly as [9],

$$\begin{aligned} W(x) &= C_1(\cos(\beta x) + \cosh(\beta x)) + C_2(\sin(\beta x) + \sinh(\beta x)) \\ &+ C_3(\cos(\beta x) - \cosh(\beta x)) + C_4(\sin(\beta x) - \sinh(\beta x)) \end{aligned} \tag{4.10}$$

On substituting this generalized solution to the spatial function in the boundary conditions, it degenerates into ω_i's corresponding to the different mode shapes of the vibrations of the cantilever beam. These frequencies are called modal frequencies. The resulting closed form solution is thus the expansion of the assumed separable solution over the modes, i.e.

$$w(x,t) = \sum_i W_i(x)\phi_i(t) \tag{4.11}$$

Now, this is with regards to the homogeneous governing equation. To solve the governing equation with an external forcing function, an expansion of the same theory is required. In general the modal frequencies derived earlier are the inherent properties of the beam and thus do not change under the influence of a force which does not permanently deform the system. Thus without loss of generality, the spatial modes can be assumed to have the same structure even when analyzing the forced vibrations. This means that one needs to reformulate the governing equations of the temporal coordinates. In this numerical analysis, it can be a computational limitation to use only a pre-specified number of modes. This in turn loads the temporal coordinates since a solution in general consisting of infinite modes is being formulated based on a few prominent ones. The convergence of solution depends on the number of modes considered. As derived in the previous chapter, to analyze

forced vibrations, let us substitute the above assumed mode expansion of the solution into the equation of motion and then using the orthogonality condition of the spatial modes, one can derive the governing equation for the temporal coordinates of the forced vibrations.

A numerically more extensive but easier to handle mathematically solution is to obtain trial functions for the spatial mode which satisfies only the essential boundary conditions and then consider more number of modes to better converge on the exact solution, there by loading the temporal coordinates extensively. This is mathematically easier to handle because in this case the spatial functions are mostly simple sinusoids. Another method is not to consider harmonic nature of spatial modes but use polynomials. This is the easiest method to handle mathematically since all the load is now on the numerical computation of the temporal modes and more the number of modes considered, convergent is the solution. For analyzing the vibrations of a cantilever beam however, it is not computationally difficult if one uses the exact spatial mode functions.

The solution to the governing equation of forced vibrations using modal analysis is discussed in the result section following the next section on FEA of the governing equation.

4.3 Finite Element Analysis of the governing EOM:

The method of modal analysis has two major limitations. Firstly the solution needs to be separable and secondly one needs to consider more number of modes for a more accurate solution which can be computationally tedious. For systems with discrete elements like a discrete damper or tip mass, the boundary conditions are non-homogeneous and thus the separation of variables fails. There is a way to work around this by modeling the discrete elements as external forcing functions with a spatial impulse functions weighing there effect at the point at which they act. This change in approach needs us to consider more modes for an accurate solution. For all these reasons, finite element method is

very effective to solve the governing equation accurately. Finite difference method using central difference formulas has been implemented in many works till now but the method suffers from the effect of artificial damping which gets introduced due to the inherent formulation of the FDM.

The FEA was first used as a solution tool as a remedy to overcome this effect of damping introduced by the FDM. In theory, the FEM is very easy to explain. Basically, the principle of the FEM is to divide the domain of interest into small elements and then express the governing equation as an integral equation over the elements and thereby solve a set of algebraic difference equations recursively over the smaller domain. The final solution is then assembled using the individual element solutions into organized system matrices. Finally, instead of solving the differential equation, we solve an equivalent algebraic matrix equation [24].

Chapter 5

VIBRATION CONTROL AND CHARACTERIZATION OF PIEZOELECTRIC MATERIALS BASED ON STATE-SWITCH TYPE SEMI-ACTIVE CONTROL LAW

5.1 Literature Review:

A state-switch concept based semi-active control scheme is proposed to enhance damping properties of piezoelectric materials [7, 8, 20]. The state-switch is related to the stiffness properties of piezoelectric materials, associating the difference between their stiffness properties in open circuit and short circuit configurations to an enhancement in the effective structural damping provided by these materials. Effectively switching the configuration of the piezoelectric sensor bonded to a cantilever beam from open circuit to short circuit when moving towards equilibrium condition and from short circuit to open circuit when moving away from the equilibrium, leads to change in stored potential energy of the system, thereby reducing the total energy. This control scheme is implemented in real time applying assumed-mode analysis for control law development. Unavailability of velocity sensors and the noise associated with numerical differentiation technique leads to the design of an output feedback variable structure observer, robust in nature and piece-wise continuous. Simulation and experimental results establish effectiveness of the vibration suppression method based on 'switched stiffness' [7].

5.2 Introduction

Active vibration control concepts are best suited for suppressing structural vibrations. However, when suppressing structural vibrations in continuous media, the effective equation of motion and their formulation involved in developing a robust enough active vibration control law is highly non-linear, thereby rendering the control law implementation computationally extensive. Also the energy of the active control inputs required for enforcing a specific damping characteristic is typically high which may lead to instability in the system under certain conditions. Intervention of noise riding

most of the feedback sensor measurements and the phase lag associated with filters implemented for noise reduction are known to cause problems in the area of vibration suppression. Another major problem associated with active control law implementation for vibration suppression in continuous media is the time delay associated with the effect of the control action taken in one section of the media to translate to the measurement points which is finitely significant [8, 18, 19]. On the other hand, passive vibration control methods are relatively simpler and have much improved stability characteristics but are less effective in vibration suppression with higher response times. To put aside the drawback of the individual methods and combine the inherent positives, hybrid methods such as adaptive passive and semi-active configurations for vibration control have been developed [18, 19].

'A recent development in this area is formulation and implementation of a state-switch based semi-active vibration control configuration. In this method, energy is dissipated by changing the effective stiffness of the system. A simple control law to effectively switch the stiffness so as to maximize the damping characteristics has been developed based on position and velocity feedbacks. The system must have effectively two stiffness values, referred to as high stiffness and low stiffness' [7, 8]. The high stiffness value is used when the system is moving away from the equilibrium condition so as to maximize the potential energy stored in the system. At the maximum amplitude of corresponding half-cycle when the potential energy stored is at its maxima, the stiffness is switched from high stiffness value to low stiffness value, dissipating the difference in the maximum potential energy proportional to the difference in the two stiffness values. Implementing this control method, the effective energy dissipated per cycles is maximized and damping characteristics of the system can be enhanced.

This energy dissipation method can be used for vibration suppression in both transient and continuously excited systems. However a functional drawback in real-time application of the state-switch control law is the requirement of accurate velocity measurements and the availability of bi-

stiffness members. To resolve the issue of expensive velocity sensors, a novel velocity observer developed by Xian et al. [22] is implemented. For vibration suppression of continuous systems, effective bi-stiffness characteristics of piezoelectric materials can be used.

5.3 Switched stiffness vibration suppression concept

It has been established that piezoelectric materials have two values for their Young's modulus of elasticity, a higher modulus of elasticity in their open circuit configuration than that in their short circuit configuration [7, 8]. Let K_{high} denote the stiffness corresponding to the open circuit configuration and K_{low} be the stiffness corresponding to the short circuit configuration. Then, the potential energy stored in the open circuit and short circuit configurations at extreme deflection is equivalent to:

$$P.E._{high} = 0.5K_{high}w_{\max}{}^2 \tag{5.1}$$

$$P.E._{low} = 0.5K_{low}w_{\max}{}^2 \tag{5.2}$$

This equivalently means that if the configuration of the piezoelectric patch is switched from open circuit to short circuit when the system moves towards equilibrium point and vice versa when system moves through the equilibrium point then per cycle of motion, an extra energy,

$$P.E. = 0.5(K_{high} - K_{low})w_{\max}{}^2 \tag{5.3}$$

can be dissipated per half cycle, thereby increasing the damping effect of the piezoelectric material.

5.3.1 Switched stiffness control law formulation

This concept of enhancing the damping properties in a system through state-switching is popularly known has Switch-Stiffness. The governing control law can be written as:

$$K(t) = K_{high}, w\dot{w} \geq 0 \tag{5.4}$$

$$K(t) = K_{low}, w\dot{w} \leq 0 \tag{5.5}$$

This can be expressed in one single equation as

$$K(t) = \left(\frac{K_{high} + K_{low}}{2}\right) + \left(\frac{K_{high} - K_{low}}{2}\right)\text{sgn}(w\dot{w}) \tag{5.6}$$

Implementing this semi-active vibration control law, one can measure the effective enhancement in the damping characteristics of the piezoelectric patch which can then be related to the enhancement in ΔK as a function of the weight ratio of nanomaterials. This experimental work can give a qualitative estimate of the coupling coefficient of the piezoelectric material which is the one of the key parameters of interest when selecting piezoelectric materials for specific applications.

5.3.2 Lyapunov-based stability analysis of the switched stiffness method

Consider the mass spring equivalent model of a distributed parameter system as

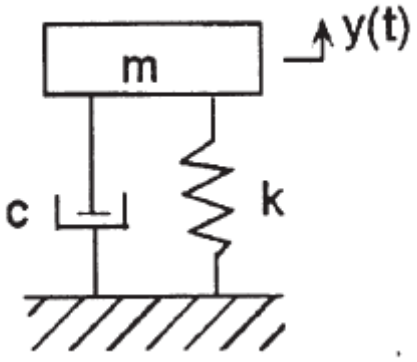

Fig 5.1 Mass-Spring-Damper equivalent of a distributed parameter system.

The governing equation of motion for this system is,

$$m(x)\ddot{y} + c(x,t)\dot{y} + k(x,t)y = 0 \tag{5.7}$$

Let us analyze the following special case:

$$\begin{cases} c(x,t) = 0 \\ k(x,t) = \left(\frac{k_{high} + k_{low}}{2}\right) + \left(\frac{k_{high} - k_{low}}{2}\right)\text{sgn}(y\dot{y}) \end{cases} \tag{5.8}$$

For this system consider the following candidate Lyapunov function

$$V = \frac{1}{2}(\dot{y}^2 + \left(\frac{k_{high} + k_{low}}{m}\right)y^2) \tag{5.9}$$

Taking the first time derivative, we have,

$$\dot{V} = -\left(\frac{k_{high} - k_{low}}{2}\right)\text{sgn}(y\dot{y}) \text{ , incorporating the system dynamics.} \tag{5.10}$$

Now, $\dot{V}$ is negative semi-definite and V is both positive definite and radially unbounded. Hence using the Invariant Set Theorem it can be proved that the system under consideration is globally asymptotically stable [14, 15, 16].

5.4 Output feedback velocity observer design

To implement the control law given by equation 5.6, a measure, observation or estimate of two states of the system, i.e. the deflection and the velocity of the free end of the beam is required. Necessarily it is not needed to have the exact values but just the signs are sufficient to effectively switch between the two configurations. Now, from the solution to the EOM one can feed-forward the value of

displacement, which will be accurate in sign. However, velocity cannot be measured directly. One solution is to use the numerical differentiation of the displacement signal to extract the sign but numerical differentiation has many problems associated with it. Hence it is necessary to either observe or estimate the velocity signal for its sign, implementing a velocity observer [10, 11, 14, 16, 21].

In state-space matrix representation, the system given by equations 5.7 and 5.8 can be expressed as

$$A = \begin{bmatrix} 0 & 1 \\ -K/m & 0 \end{bmatrix}, C = [10] \tag{5.11}$$

We suggest the following structure of a full state observer:

$$\dot{\hat{x}} = A\hat{x} - L\tilde{y} \tag{5.12}$$

where, L is the state feedback gain matrix to be designed for desired positioning of observer poles, and $\tilde{y}$ is measure of observer error. Let

$$L = \begin{bmatrix} K_1 \\ K_2 \end{bmatrix} \tag{5.13}$$

This completes the observer design to be

$$\dot{\hat{y}} = p + K_1\tilde{y} \tag{5.14}$$

$$\dot{p} = -\frac{K}{m}y + K_2\tilde{y} \tag{5.15}$$

Note that this observer design is in the structure of a second order filter.

Now let us examine the stability of this design. For this, let's obtain the error dynamics. The observer error is given by

$$\tilde{y} = y - \hat{y} \tag{5.16}$$

Thus,

$$\dddot{\tilde{y}} = \ddot{y} - \dddot{\hat{y}} = -\frac{k}{m}\dot{y} - \dot{p} - K_1\ddot{\tilde{y}} \tag{5.17}$$

It can be seen that we need to redesign the observer for both stable and converging nature desired of the observer. We now suggest the following structure, retaining the second order filter design.

$$\dot{\hat{y}} = p + K_1\tilde{y} \tag{5.18}$$

$$\dot{p} = -\left(\frac{\left(\frac{k_{high}+k_{low}}{2}\right) + 2\left(\frac{k_{high}-k_{low}}{2}\right)\mathrm{sgn}\left(y\dot{\hat{y}}\right)}{m}\right)y + K_2\tilde{y} \tag{5.19}$$

Using this design, the error dynamics can be rewritten as:

$$\dddot{\tilde{y}} = \frac{\left(\frac{k_{high}-k_{low}}{2}\right)\mathrm{sgn}\left(y\dot{\hat{y}}\right)}{m}y - K_2\tilde{y} - K_1\ddot{\tilde{y}} \tag{5.20}$$

Consider the following candidate Lyapunov function to analyze the stability of the design.

$$V = \frac{1}{2}\dot{y}^2 + \frac{k_{high}+k_{low}}{2m}y^2 + \frac{1}{2}\ddot{\tilde{y}}^2 + \frac{K_2}{2}\tilde{y}^2 \tag{5.21}$$

Differentiating with time and incorporating the error dynamics, we get

$$\dot{V} = -\frac{(k_{high} - k_{low})}{2m} y\dot{\hat{y}}\,\mathrm{sgn}\left(y\dot{\hat{y}}\right) - K_1\dot{\tilde{y}}^2 \tag{5.22}$$

Now, $\dot{V}$ is negative semi-definite and V is radially unbounded [20, 21]. Thus using the Invariant Set Theorem [20, 21], it can be proved that the overall system with the defined control law and the refined observer design is globally asymptotically stable.

5.5 Characterization of piezoelectric materials (Mathematical Modeling)

Consider the homogeneous equation of motion of a cantilever beam which is given by:

$$\rho A(x)\frac{\partial^2 w(x,t)}{\partial t^2} + \frac{\partial^2}{\partial x^2}\left(EI(x)\frac{\partial^2 w(x,t)}{\partial x^2}\right) = 0 \tag{5.23}$$

Let this cantilever beam have a PZT patch bonded to it which acts just as a sensor. Now let us analyze the motion under vibrations induced only because of initial conditions. As a function of the displacement of the vibrations, the charge accumulating on the PZT patch is given by

$$Q = 0.5bE^s d_{31s}(l_2 - l_1)\left(\frac{\partial w(l_2,t)}{\partial x} - \frac{\partial w(l_1,t)}{\partial x}\right) \tag{5.24}$$

where, E^s is the Young's modulus of electricity of the sensor material and d_{31s} is the piezoelectric constant of the sensor.

Initially there is no voltage applied to the patch which is acting only as a sensor. However, the sensor being a potential parallel plate capacitor, charge developed on it will produce output voltage that can be sensed. Now since the patch is bonded to the beam this voltage can be seen as an excitation signal applied to the beam. This is the source of the electromechanical coupling in the piezoelectric material. Depending on the sign of the voltage and the charge accumulating on the

patch, the motion of the beam will be altered and this can be seen as the source of the vibration damping characteristics of the piezoelectric sensors. Therefore the charge developing on the patch can be rewritten to incorporate the electromechanical coupling effect.

$$Q = 0.5bE^{s}d_{31s}(l_2 - l_1)(\frac{\partial w(l_2,t)}{\partial x} - \frac{\partial w(l_1,t)}{\partial x}) + \frac{\varepsilon v(t)}{t_p}A \quad \text{where 'A' is the area of the patch.} \qquad (5.25)$$

This equation can also be written from the constitutive equations of piezoelectricity considering the effect of the field produced by voltage applied to the patch. When one analyzes forced vibrations, the effect of sensed voltage is negligible compared to the order of the applied voltage but in the analysis of vibrations induced due to initial conditions, incorporating this effect may give us some added insight.

Now, from equation 5.25,

$$v(t) = \frac{0.5bE^{p}d_{31}(l_2 - l_1)\left(\left(\frac{\partial w(l_2,t)}{\partial x}\right) - \left(\frac{\partial w(l_1,t)}{\partial x}\right)\right)}{C_p\left(1 - \frac{\varepsilon A}{t_p C_p}\right)} = \frac{0.5E^{p}d_{31}(volume)}{t_p C_p - \varepsilon A}\left(\left(\frac{\partial w(l_2,t)}{\partial x}\right) - \left(\frac{\partial w(l_1,t)}{\partial x}\right)\right) \qquad (5.26)$$

which gives the net voltage that can be seen as externally applied to the piezoelectric patch when analyzing vibrations due to initial conditions. Thus going back and reforming our equation of motion as:

$$\rho A(x)\frac{\partial^2 w(x,t)}{\partial t^2}+\frac{\partial^2}{\partial x^2}\left(EI(x)\frac{\partial^2 w(x,t)}{\partial x^2}\right)= \\ \frac{\partial^2}{\partial x^2}\left(\frac{-0.5bE^{p2}{d_{31}}^2(l_2-l_1)s(x)(volume)}{t_pC_p-\varepsilon A}\left(\left(\frac{\partial w(l_2,t)}{\partial x}\right)-\left(\frac{\partial w(l_1,t)}{\partial x}\right)\right)\right) \tag{5.27}$$

Assuming that a solution to this non-linear partial differential equation exists and that the *x*-coordinate is separable from the temporal coordinate, let us assume the solution to be in the assumed mode expansion given by,

$$w(x,t)=\sum_i W_i(x)q_i(t) \tag{5.28}$$

Substituting the assumed mode expansion of the solution in the equation of motion, we have:

$$\sum_i\left(\rho A(x)W_i(x)\ddot{q}_i+\frac{\partial^2}{\partial x^2}\left(EI(x)W_i^{''}(x)\right)q_i\right)= \\ \sum_i\left(\frac{\partial^2}{\partial x^2}\left(\frac{-0.5bE^{p2}{d_{31}}^2(l_2-l_1)s(x)(volume)}{t_pC_p-\varepsilon A}\right)\left(W_i^{'}(l_2)-W_i^{'}(l_1)\right)q_i\right) \tag{5.29}$$

Multiplying both sides of the equation by $W_j(x)$ and integrating over the domain, one can use the orthogonality condition of the modes to reform the equations. Thus we have:

$$\ddot{q}_i+\omega_i^2 q_i=B_i q_i\int_0^l\left(\frac{\partial^2}{\partial x^2}s(x)\right)W_i(x)\,dx \tag{5.30}$$

where, $B_i=\left(\frac{-0.5bE^{p2}{d_{31}}^2(l_2-l_1)(volume)}{t_pC_p-\varepsilon A}\right)\left(W_i^{'}(l_2)-W_i^{'}(l_1)\right)$

and $\omega_i=((2i-1)\frac{\pi}{2})^2\left(\frac{EI}{\rho Al^4}\right)^{0.5}$

Let $N_i = \int_0^l (\frac{\partial^2}{\partial x^2} s(x)) W_i(x)\, dx$ (5.31)

Integrating by parts, we have

$$N_i = \frac{dW_i(l_2)}{dx} - \frac{dW_i(l_1)}{dx} \tag{5.32}$$

Thus we have

$$\ddot{q}_i + (\omega_i^2 - (B_i N_i)) q_i = 0 \tag{5.33}$$

as the governing equation of the temporal coordinates.

It is observed that the natural frequency of vibrations in the temporal coordinate is shifted. It is easy to establish that the sign of the product '*BI*' is negative and hence the shift in frequency is towards the higher side. Now, ω_i is the frequency of mechanical vibrations, the natural frequency corresponding to the ith mode. The shift in this frequency is observed after considering the effect of the electromechanical coupling and incorporating it into the equations of motion.

Using the governing equations derived in 5.33, let us now discuss the implementation of the Switch-Stiffness control law. Using the governing equation for the temporal coordinates and implementing the observer for every coordinate function, the exact sign of the product $w\dot{w}$. However, for this it is needed to separate the initial condition, *w(x,0)* on to the initial conditions of the temporal coordinates of each mode. Let us now discuss this last piece of work towards the complete characterization.

For this, consider the homogeneous equation of motion given by equation 5.23. Assume the solution to this EOM to be in the form of a closed loop assumed mode expansion given by equation 5.28. For a given initial condition, *w(x,0)*, have

$$w(x,0) = \sum_i W_i(x)\, q_i(0) \tag{5.34}$$

$$\rho A(x) w(x,0) = \sum_i \rho A(x) W_i(x)\, q_i(0) \tag{5.35}$$

$$\int_0^l \rho A(x) w(x,0) W_j(x)\, dx = \sum_i \int_0^l q_i(0) \rho A(x) W_i(x) W_j(x)\, dx \tag{5.36}$$

Applying the orthogonality condition of the modes, we have

$$q_i(0) = \int_0^l \rho A(x) w(x,0) W_i(x)\, dx \tag{5.37}$$

Similarly,

$$\dot{q}_i(0) = \int_0^l \rho A(x)\, \dot{w}(x,0) W_i(x)\, dx \tag{5.38}$$

Using this one can distribute the initial condition of motion on all the modes considered. Combining with this with the discussion on the shift in frequency observed, the implementation designed is shown in figure 5.2

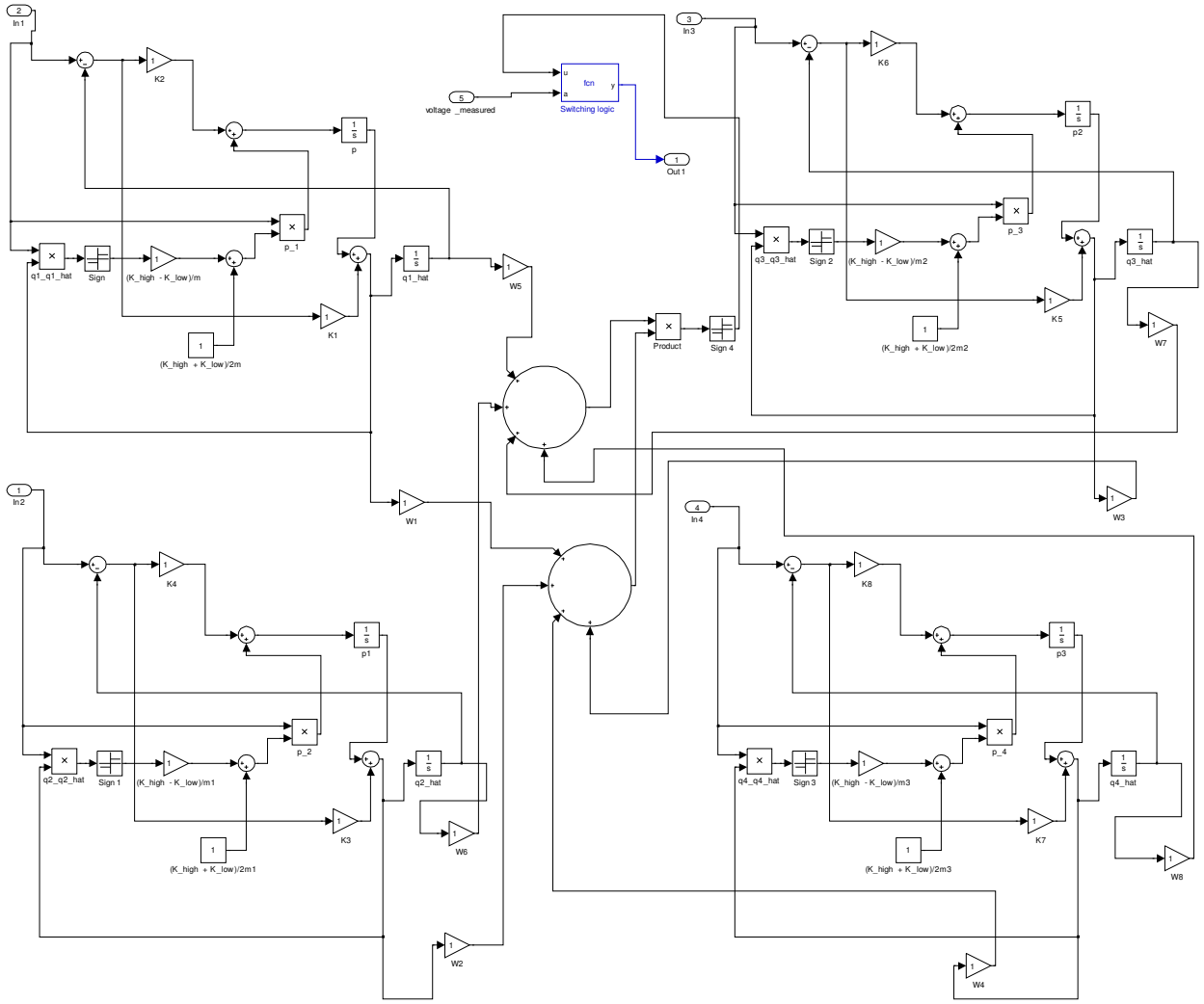

Fig.5.2 Simulink model for implementation of switched stiffness control law.

5.6 Discussion of results

5.6.1 Simulation results implementing the velocity observer

To obtain the velocity feedback required to implement the switched stiffness control law developed in Section 5.2, an output feedback velocity observer has been designed. In this section let us discuss the results obtained by implementing this observer design. Figure 5.3(a) plots the actual position measured and the observed position. As can be seen the observer's estimate of position is not in accordance with the measured position in terms of magnitude, but the observed signal follows the same sign which is the key factor in implementing the switched stiffness control law.

A similar observation can be made between the actual velocity of simulation signal and its observer signal. This comparison is presented in Figure 5.3(b). It can be seen that even though the observer does not observe the exact signal, the sign of the actual signal and the observed signals match accurately.

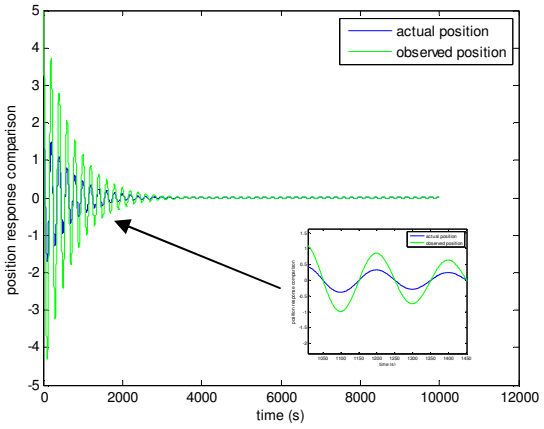

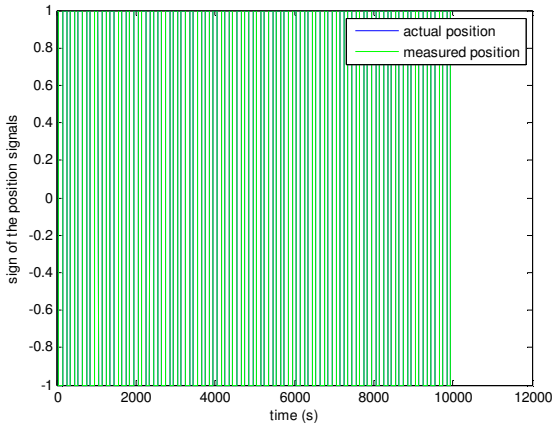

(a)

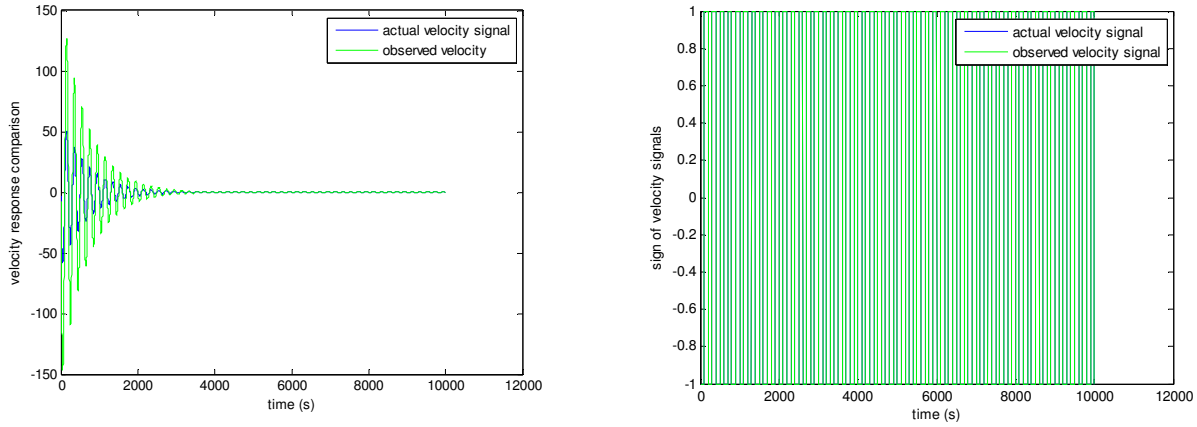

(b)

Fig. 5.3 (a) Comparison of measured and observed position signals and their signs and (b) Comparison of measured and observed velocity signals and their signs.

5.6.2 Experimental results and discussion

The switched stiffness formulation developed in Section 5.2 has been implemented in real time incorporating the output feedback state observer in the control law to suppress vibration induced by initial conditions in a cantilever beam fixed at one end and free at the other. A sensor fabricated from piezoelectric polymers such as PVDF and PAN is used as the bi-stiffness member and the configuration of this member is changed between open circuit and short circuit through a novel software switching code. The experimental bench is shown Figure 5.4.

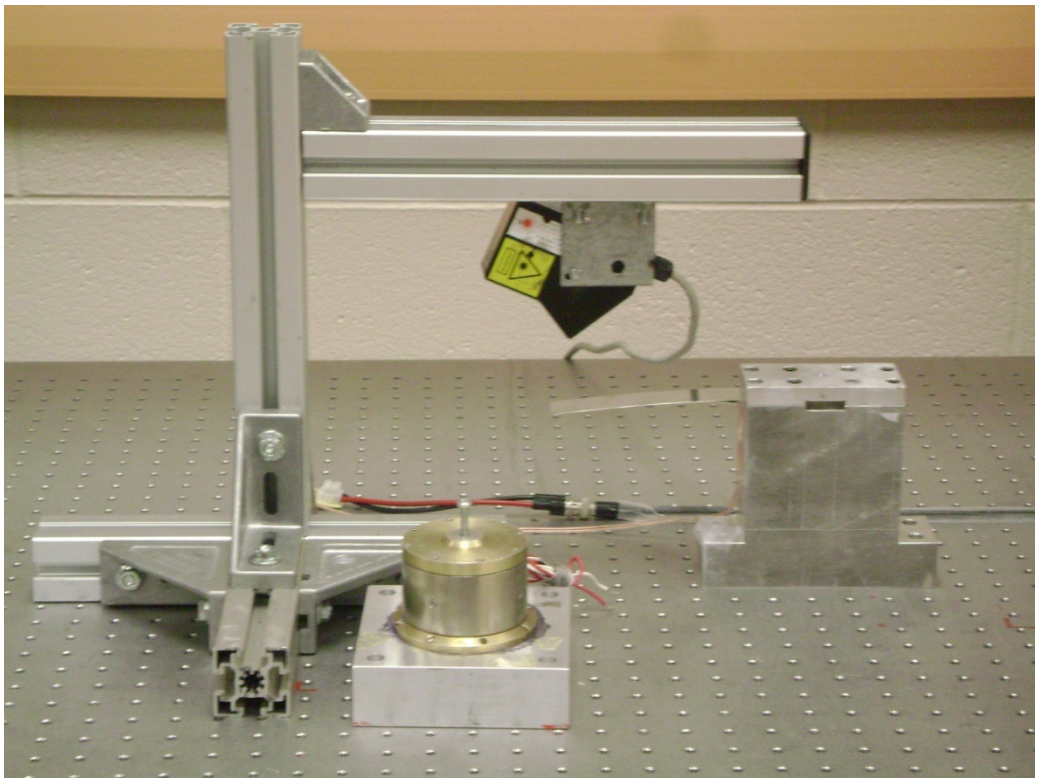

Fig. 5.4. Experimental bench

The results of the experiment conducted are tabulated below.

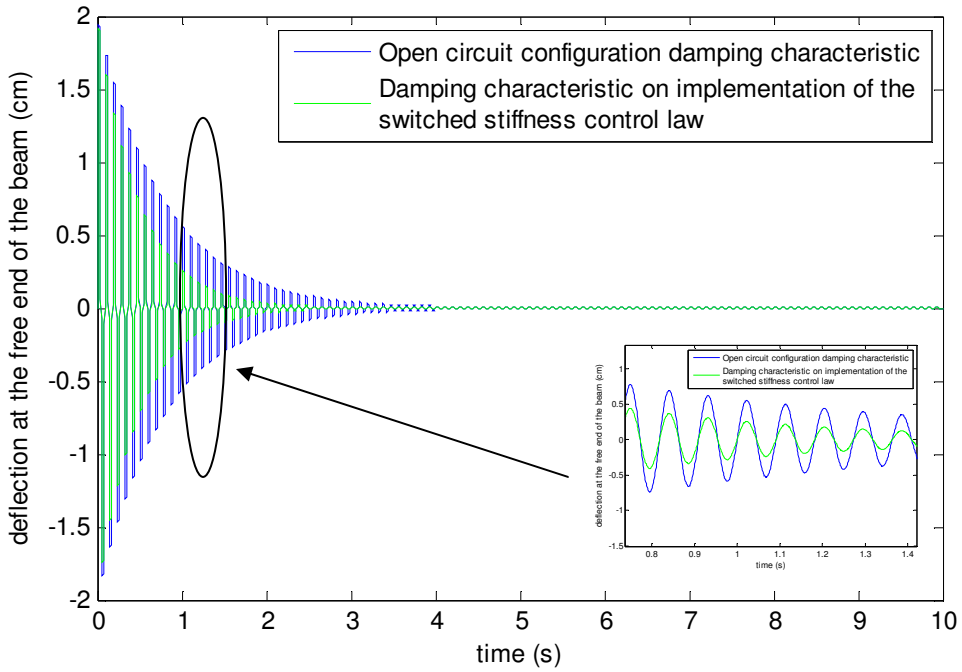

(a)

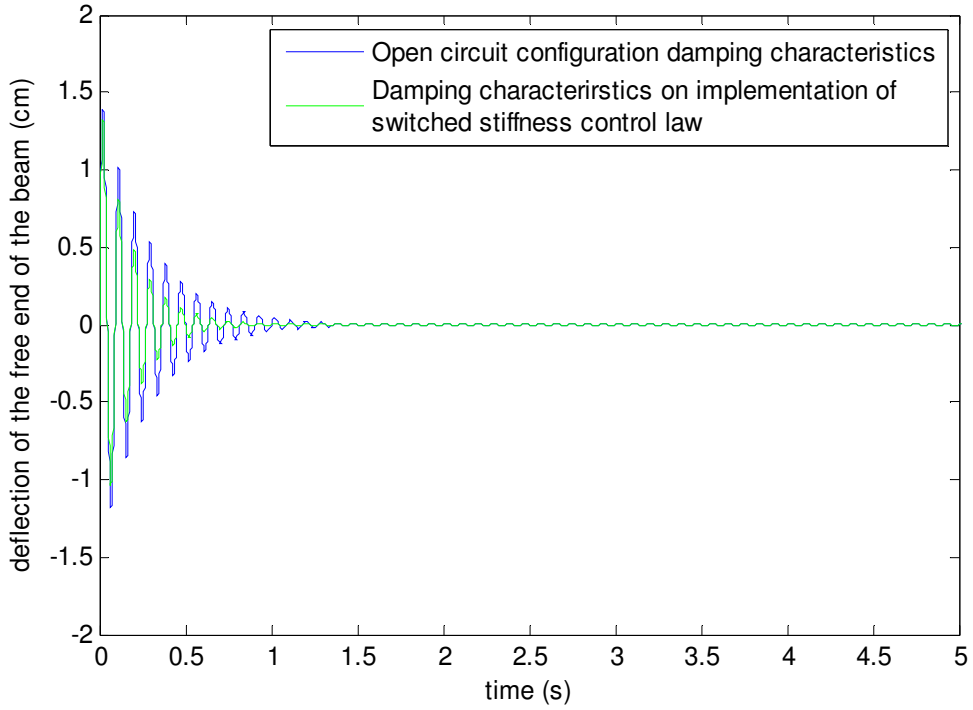

(b)

Fig.5.5 (a) Experimental response of the free end of the beam for initial condition induced vibrations with fabric sensor fabricated from pure PVDF bonded to the beam and (b) Experimental response of the free end of the beam for initial condition induced vibrations with fabric sensor fabricated from pure PVDF and 0.25% SWNTs bonded to the beam.

From the above results it is clearly seen that the switched stiffness control law proposed for semi-active vibration suppression enhances the damping characteristics of the pzt sensor material. Also, it can be seen, addition of SWNTs to the mother solution of the polymer enhances the piezoelectric properties of the fabric sensor.

5.7 Results for characterization of piezoelectric materials

Developing on the analysis performed in Section 5.5, a formulation for the estimate of the coupling coefficient, k_{31} [25] is proposed based on the observation of the associated frequency shift which is now a function of both the electrical mode as well as the mechanical mode,

$$k_{31} = \frac{\omega_i - \left|\omega_i - \sqrt{\left|B_i N_i\right|}\right|}{\omega_i}, i = 1 \tag{5.39}$$

For the ease of this estimation the following lookup table has been developed, based on the numerical values of the mechanical properties of the actual experimental bench.

Lookup Table 5.1. (l_1=10mm, l_2=50mm)**:**

Serial No. (i)	ω_i **(Hz)**	N_i
1	10	-2.2056
2	85.51	-11.1321
3	251.7	-11.9237
4	569.63	9.3053

The results of this section are discussed in table 5.1.

Table 5.1. Results for the estimation of the coupling coefficient k_{31} and its comparison with literature values for validation.

Serial No.	**Type of sensor attached**	**Natural Frequency of beam in first mode, calculated. (hz)**	**Natural Frequency of first mode observed in experimental mode. (hz)**	**Calculated k_{31}**	**Theoretical k_{31}**
1	Commercial PZT patch	10	16.8	0.32	0.35
2	PVDF	10	19	0.0875	0.11
3	PVDF with 0.1% SWNTs	10	18.5	0.1535	
4	PVDF with 0.25% SWNTs	10	18	0.2105	

Chapter 6

EQUIVALENT STRUCTURAL DAMPING MODEL: DESIGN AND IMPLEMENTATION OF AN ACTIVE VIBRATION SUPPRESSION SCHEME

6.1 Literature Review and Introduction

As discussed in the last chapter, the switched stiffness vibration suppression scheme is a semi-active vibration suppression method which exploits the bi-stiffness property of piezoelectric materials to add structural damping to a continuous member [12, 13]. This concept has been modeled extensively in the last chapter. This chapter expands the discussion further and looks into whether we can model the same vibration damping law as an active vibration suppression method. This work is based completely on the energy method of deriving equations of motions, using the extended Hamilton's principle [9].

As seen in the last chapter, the switched stiffness concept dissipates energy equivalent to the maximum vibration amplitude every cycle. The bi-stiffness property of the piezo-sensor allows us to switch between the two configurations using computer software. Now the proposed real time implementation requires a velocity observer which is really difficult to implement on continuous systems. For continuous systems, real time analysis of the continuous EOM with just the tip displacement to observe tip velocity has the limitation of mode expansion. Also the modal method introduces a significant software delay and thus the switching cannot be perfectly synchronized. As a result even though the vibrations may go close to zero for sometime but the delays may act up as actuators as seen from the experimental results. Thus the damping scheme is not smooth and sudden shoot up as a result of actuation is not acceptable.

Proposed is this discussion is the expansion of the semi-active vibration suppression method into an active one. Modeling the energy dissipation per cycle as energy dissipated by an equivalent discrete damper, a new set of governing equations with an explicit damping term which reflects as an external

force is derived. This enables us to design a control voltage to functionalize the piezo-sensor as an actuator to apply active voltage equivalent to the damping characteristics of the switched stiffness concept. This actuation eliminates the software delays and a clean exponential damping characteristic is verified experimentally.

From the example of classical SDOF systems, the dissipative energy function for structural damping in the Lagrangian or Hamilton's principle method of obtaining the governing equations is given by:

$$D = \int_0^l \frac{1}{2} c_{eq} \dot{w}_x dx \tag{6.1}$$

where c_{eq} is the equivalent structural damping coefficient [10].

The energy dissipated per cycle can be modeled to fit this structural damping energy term and the equivalent damping coefficient can be established. This equivalence then needs to be verified by extensive numerical simulations and finally experimental results. This in general is the layout of this, the penultimate chapter.

6.2 Mathematical modeling of the switch stiffness control logic as equivalent dissipated energy:

As per the switch stiffness concept introduced and explained in the last chapter, the variable stiffness of the system can be written is one single equation as:

$$k(t) = \left(\frac{k_{high} + k_{low}}{2} \right) + \left(\frac{k_{high} - k_{low}}{2} \right) \operatorname{sgn}\left(w\dot{w} \right) \tag{6.2}$$

The energy stored in this varying stiffness is the dissipated energy per cycle. This average energy dissipated per vibration cycle can be modeled as:

$$E = \frac{1}{T} \int_0^T \int_{domain} k(t) w \frac{\partial w}{\partial x} dx dt \tag{6.3}$$

Without loss of generality we can assume that at t = 0, the beam is at equilibrium position moving away from it. Under this valid assumption, the average energy dissipated per vibration cycle is given by,

$$E = \frac{1}{T}\left\{ \int_0^{T/4}\int_{l_1}^{l_2} k_{high} w \frac{\partial w}{\partial x} dxdt + \int_{T/4}^{T/2}\int_{l_1}^{l_2} k_{low} w \frac{\partial w}{\partial x} dxdt + \int_{T/2}^{3T/4}\int_{l_1}^{l_2} k_{high} w \frac{\partial w}{\partial x} dxdt + \int_{3T/4}^{T}\int_{l_1}^{l_2} k_{low} w \frac{\partial w}{\partial x} dxdt \right\} \quad (6.4)$$

i.e.

$$E = \frac{1}{2T}\left\{ \int_0^{T/4} k_{high} \left[w^2 \right]_{l_1}^{l_2} dt + \int_{T/4}^{T/2} k_{low} \left[w^2 \right]_{l_1}^{l_2} dt + \int_{T/2}^{3T/4} k_{high} \left[w^2 \right]_{l_1}^{l_2} dt + \int_{3T/4}^{T} k_{low} \left[w^2 \right]_{l_1}^{l_2} dt + \right\} \quad (6.5)$$

Extending the concept of the equivalent energy dissipated by a discrete structural damper from SDOF systems to continuous systems, the energy dissipated by an equivalent structural damper can be written as,

$$E_d = \frac{1}{T}\int_0^{T}\int_{l_1}^{l_2} c_{eq} \frac{\partial^2 w}{\partial t \partial x} dxdt \quad (6.6)$$

where, c_{eq} is the equivalent structural damping coefficient [10].

The equivalent structural damping coefficient is a term that we have introduced to model the original semi-active vibration suppression scheme into an active vibration suppression scheme. This structural damping coefficient is established through the equivalence of the energy dissipated. Equivalent to the average energy dissipated over one vibration cycle as given by equations 6.5 and 6.6, comparing the energy dissipated over one half cycle,

$$\frac{c_{eq}(\dot{w}_{\max})^2 T}{4} = \frac{\Delta k (w_{\max})^2}{2} \quad (6.7)$$

i.e.

$$c_{eq} = 2\Delta k \frac{\left(w_{\max}(L)\right)^2}{T \cdot (\dot{w}_{\max}(L))^2} \tag{6.8}$$

Without loss of generality we can assume an exponential decay in the vibration amplitude of the free end of the beam, which is the only point of measurement, we have

$\dot{w}_{\max}(L) = -\lambda w_{\max}(L)$, where λ is the logarithmic decay ratio. (6.9)

Therefore, the equivalent damping coefficient is given by,

$$c_{eq} = \frac{2\Delta k}{T\lambda^2} \tag{6.10}$$

As seen, the equivalent damping coefficient depends on three important factors; the difference between the higher and lower stiffness values for the piezo-patch, the period of vibrations and the logarithmic decay ratio. Developing our theory further based on this established equivalence, let us now derive the new set of governing equations with the structural damping equivalence as an external forcing function.

6.3 Mathematical modeling of the new set of governing equations:

The kinetic energy and the strain (potential) energy of the beam under vibrations as derived in chapter 3, is given by,

$$T = \int_0^l \rho A(x)(\frac{\partial w}{\partial t})^2 dx \tag{6.11}$$

$$\Pi = \int_0^l EI(x)(\frac{\partial^2 w}{\partial x^2})^2 dx \tag{6.12}$$

Based on the expression of energy dissipated in a structural damper for SDOF systems, the external forcing function which is the equivalent energy dissipation in the structural damping model, is given by

$$W = \int_0^l c_{eq} s(x) \frac{\partial^2 w}{\partial t \partial x} dx \tag{6.13}$$

Applying the generalized Hamiltonian principle, we have

$$\int_{t_1}^{t_2} \delta(\Pi - T - W) dt = 0 \tag{6.14}$$

The variation on the kinetic and potential energy terms has been performed extensively in the discussion in chapter 3. Here let us discuss the variation on the external forcing function.

$$\begin{aligned} \int_{t_1}^{t_2} \delta W dt &= \int_0^l \int_{t_1}^{t_2} c_{eq} s(x) \frac{\partial}{\partial t} \frac{\partial(\delta w)}{\partial x} dt dx + \int_{t_1}^{t_2} \int_0^l c_{eq} s(x) \frac{\partial}{\partial x} \frac{\partial(\delta w)}{\partial t} dx dt \\ &= -\int_{t_1}^{t_2} \int_0^l \frac{\partial}{\partial t}\left(c_{eq} s(x) \frac{\partial w}{\partial x} \right) \delta w dx dt - \int_{t_1}^{t_2} \int_0^l \frac{\partial}{\partial x}\left(c_{eq} s(x) \frac{\partial w}{\partial t} \right) \delta w dx dt \end{aligned} \tag{6.15}$$

Substituting this in equation (), we obtain the governing equation

$$\rho A(x) \frac{\partial^2 w}{\partial t^2} + \frac{\partial^2}{\partial x^2}\left(EI(x) \frac{\partial^2 w}{\partial x^2} \right) = -\left\{ \frac{\partial}{\partial t}\left(c_{eq} s(x) \frac{\partial w}{\partial x} \right) + \frac{\partial}{\partial x}\left(c_{eq} s(x) \frac{\partial w}{\partial t} \right) \right\} \tag{6.16}$$

This new governing equation has the same original fixed-free boundary conditions associated with it.

From the governing equation of a piezoelectric actuator as derived in chapter 3, we have

$$\rho A(x) \frac{\partial^2 w(x,t)}{\partial t^2} + \frac{\partial^2}{\partial x^2}\left(EI(x) \frac{\partial^2 w(x,t)}{\partial x^2} \right) = \frac{\partial^2}{\partial x^2}\left(-0.5 b E^p d_{31} v(t) \left(t_p + t_b - 2 z_n \right) s(x) \right) \tag{6.17}$$

The governing equation given by equation 6.16 has to be now modeled as the governing equation 6.17 by designing a control voltage which dictates the same energy over one vibration cycle as the energy dissipated per cycle by the structural damping structure, i.e.

$$\int_t \int_0^l c_{eq} s(x) \frac{\partial^2 w}{\partial t \partial x} dx dt = \int_t \int_0^l B \cdot s(x) v(t) \frac{\partial^2 w}{\partial x^2} dx dt \quad \text{, where } B = \frac{b}{2} \cdot 0.5 E^P d_{31} \left(t_p + t_b - 2 z_n \right) \tag{6.18}$$

Design of the control voltage *v(t)* from the above integral equation is mathematically tedious without the knowledge of the structures of the signals involved in the integrand. To simplify this issue, lets obtain the numerical solution to the governing equation with structural damper as an external forcing function. The solution to the governing equation derived using FEA [24], which will be in terms of c_{eq}, can be used to compare the solution to the actuator equation and that of the equivalent damping model, and thereby design a compensating structure for the voltage *v(t)*. The analysis from here on is purely numerical and computational.

6.3.1 Modal analysis of the new governing equation set:

As discussed above, the new set of governing equations has the same fixed-free boundary conditions associated with it. Thus the spatial shape function or mode shape will not change in fundamental mathematical formulation. Substituting the assumed mode solution in its expanded form in the governing equation, we have

$$\sum \begin{Bmatrix} \rho A(x) W_i(x)\ddot{q}_i(t) + \dfrac{\partial^2}{\partial x^2}\left(EI(x)W_i''(x)q_i(t)\right) + 2c_{eq}s(x)W_i'(x)q_i(t) + \\ c_{eq}\cdot\dfrac{\partial}{\partial x}s(x)W_i(x)\dot{q}_i(t) + s(x)W_i'(x)q_i(t)\dfrac{\partial c_{eq}}{\partial t} \end{Bmatrix} = 0 \qquad (6.19)$$

Multiplying throughout by $W_j(x)$, and applying the orthogonality conditions of the mode shapes of a Euler-Bernoulli beam [9], the governing equation for the ith temporal coordinate is obtained as,

$$\begin{aligned} &\ddot{q}_i(t)\int_0^l \rho A(x)W_i(x)W_j(x)dx + q_i(t)\int_0^l EI(x)W_i''W_j''dx + \dot{q}_i(t)\int_0^l c_{eq}\frac{\partial s(x)}{\partial x}W_i'W_j'dx \\ &+\dot{q}_i(t)\int_0^l 2c_{eq}s(x)W_i'W_j\,dx + q_i(t)\int_l^{l_2} W_i'W_j\,\frac{\partial c_{eq}}{\partial t}dx = 0 \end{aligned} \qquad (6.20)$$

i.e.

$$\ddot{q}_i(t)+\omega_i^2 q_i(t)+\dot{q}_i(t)\int_0^l c_{eq}\frac{\partial s(x)}{\partial x}W_i^{'}W_j^{'}dx$$
$$+\dot{q}_i(t)\int_0^l 2c_{eq}s(x)W_i^{'}W_j\,dx+q_i(t)\frac{\partial c_{eq}}{\partial t}\int_l^{l_2} W_i^{'}W_j\,dx=0 \qquad (6.21)$$

6.4 Discussion of Results:

6.4.1 Numerical Simulation: Validation of equivalent damping model:

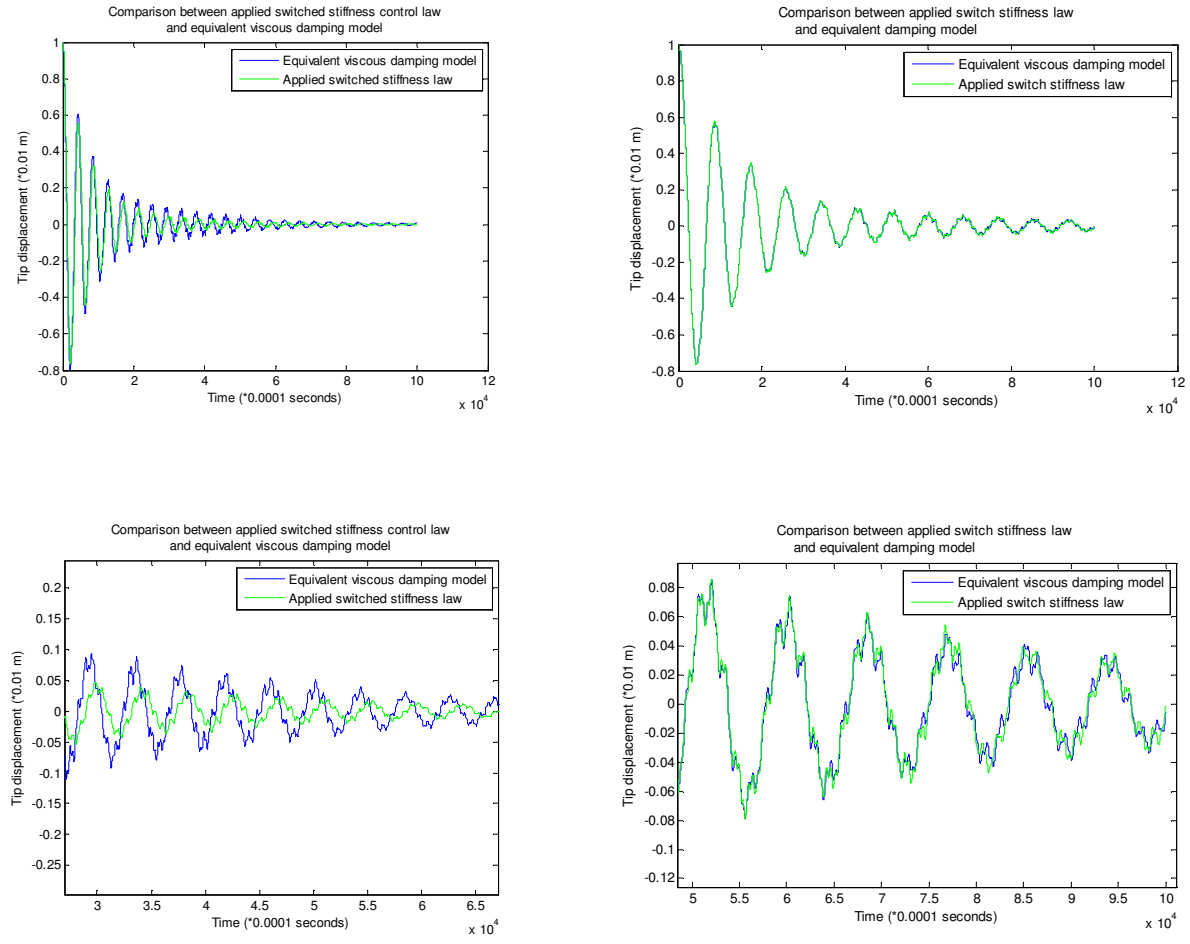

Figure 6.1 Numerical simulation for validation under two different sets of beam specifications

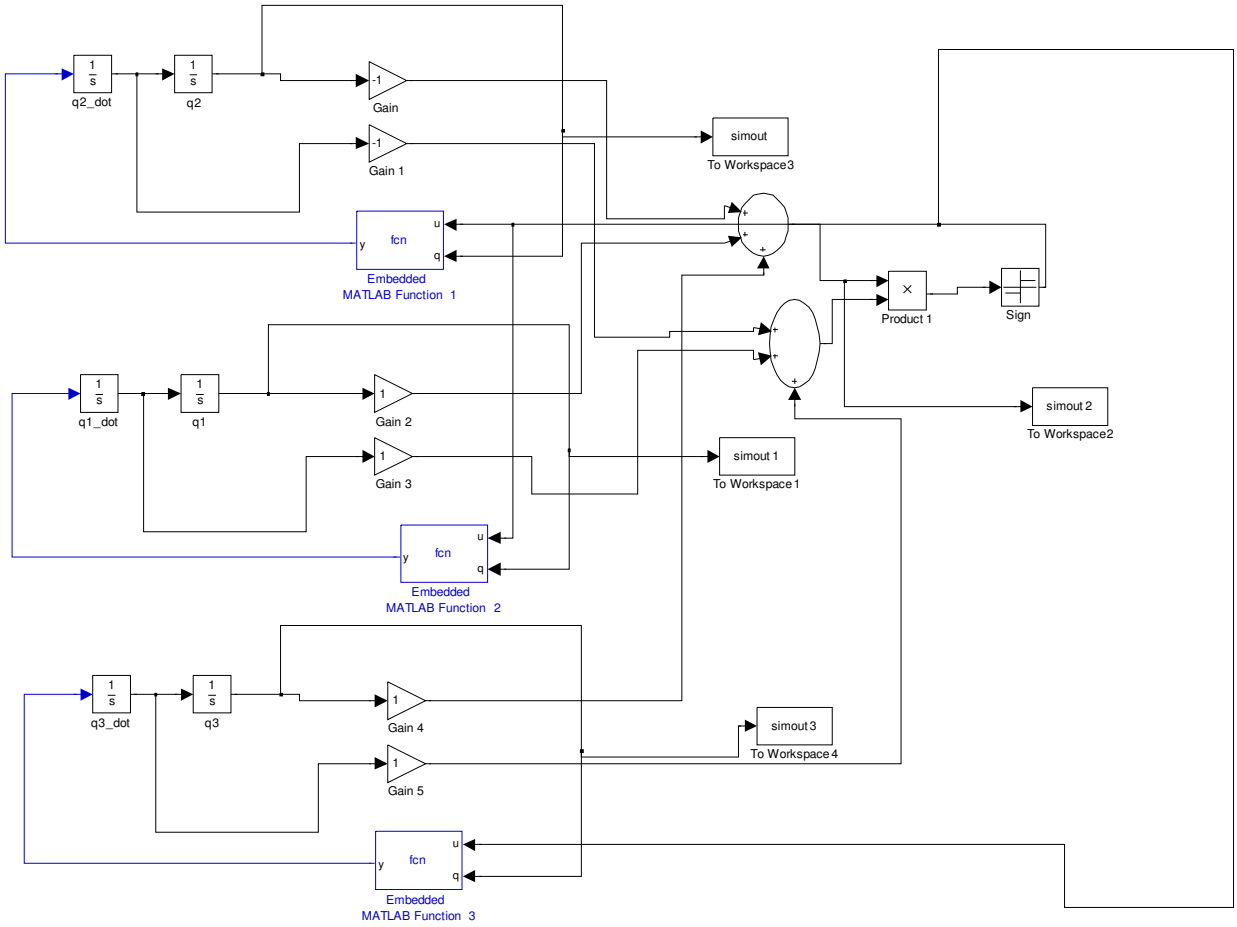

Figure 6.2 Simulink based model layout to validate equivalent damping model.

As seen from the tabulation of results in Figure 6.1, it is seen that the equivalent damping model developed and proposed in this work is accurate enough for beams with lower first natural frequencies. The proposed model however disintegrates for beams with higher first natural frequencies as compared to the actual switch stiffness control law. This is due to the period dependence of the equivalent structural damping coefficient [10, 12]. As the period of vibration reduces, the decay ratio is not exactly logarithmic, implying the decay is not exponential. This is not in accordance with the exponential decay assumption which forms the base of the derived mathematical equivalence of the structural damping coefficient. This is however as far as we discuss

this mathematical tool in the scope of this thesis. In the concluding remarks made in the final chapter, future work in this area is discussed.

6.4.2 Application of Switched Stiffness control law using the equivalent structural damping model and its comparison versus implementation of the semi-active vibration suppression method:

Extending the concept of the semi-active vibration suppression scheme of switched stiffness to the concept of equivalent structural damping, the damping effect of the scheme was modeled as equivalent damping energy and a structural damping term equivalent to the piezoelectric effect was introduced to implement an active vibration damping scheme by designing appropriate voltage signal to the piezoelectric actuator which overcomes the inherent delay introduced due to the instrumentation in the semi-active vibration suppression scheme. The result of this work is a much sharper and faster exponential decay.

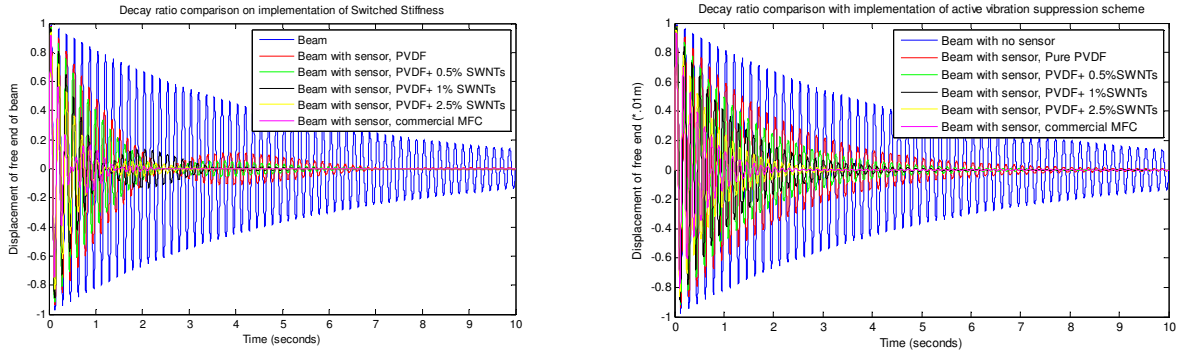

Figure 6.3 Comparison between applied switched stiffness control logic and equivalent damping model based active vibration control characteristics.

When applying the semi-active vibration suppression scheme, there is finite and significant delay involved in the mathematical processing of the tip displacement measured using the laser vibrometer principle. This delay results in the soft switching logic developed not being synchronized with the exact change in the sign of the product, '$w\dot{w}$'. As a result sometimes instead of removing energy from the system, the logic may actuate the system due to the switching not being in sync. This is seen

in the above tabulation of primary results. The Figure 6.4 is the simulink model developed to implement the switch stiffness vibration suppression method.

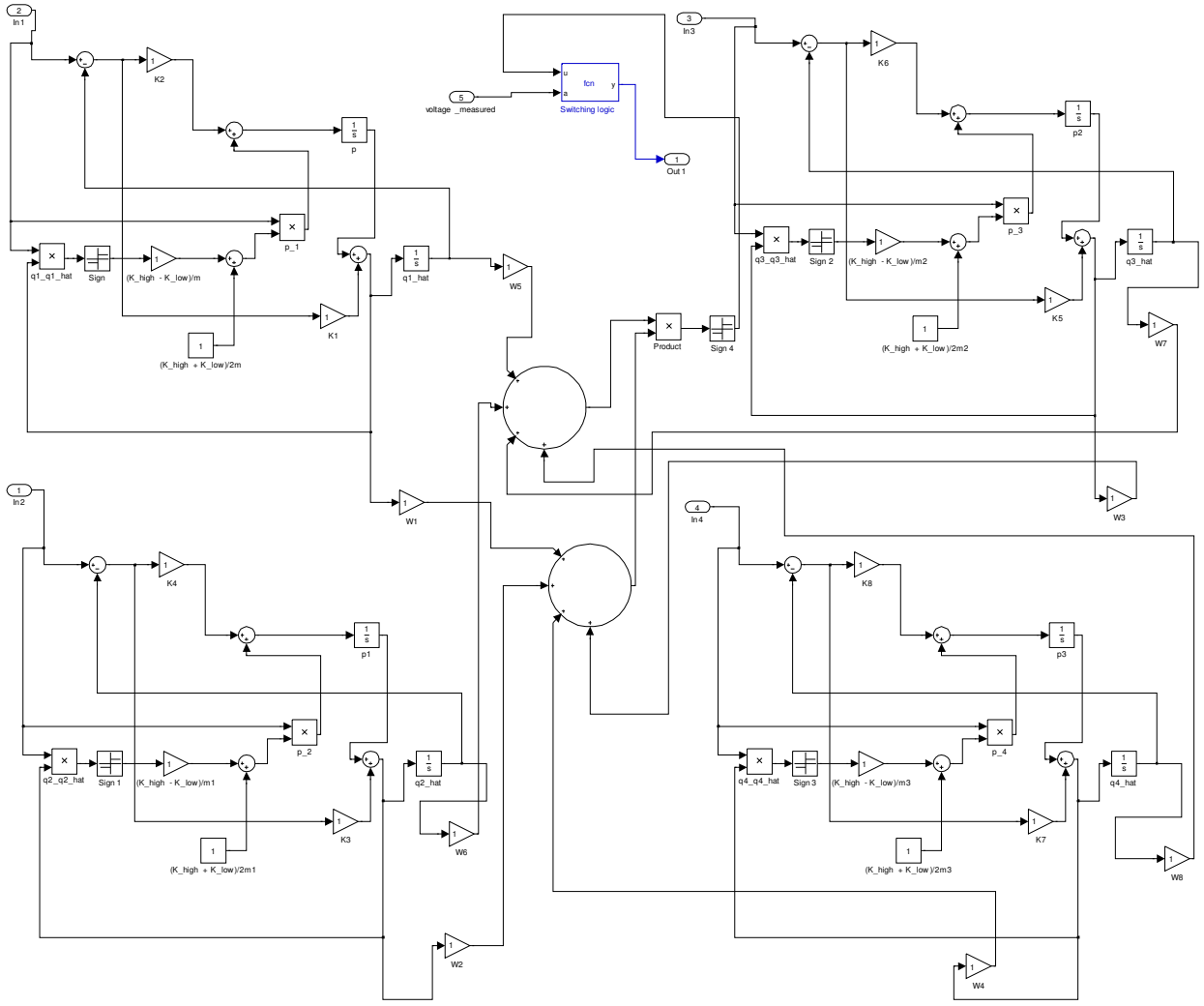

Figure 6.4 Simulink based model layout to implement the switched stiffness control law.

6.5 Characterization of piezoelectric materials, a summary of results:

Chapter 5 discusses the formulation and implementation of the state-switch based semi active control law. Based on the mathematical modeling a novel formulation of the coupling coefficient, k_{31} [21, 25], has been proposed and validated. Here, let us discuss the decoupling of the mechanical and electrical properties of the piezoelectric materials based on this coupling coefficient model.

6.5.1 Piezoelectric Constant g_{ij}

"The piezoelectric coefficient g_{ij} denotes the electric field developed along i-axis (electrodes perpendicular to i-axis) due to an applied stress along j-axis provided all other external stresses are constant. It also expresses the strain developed along j-axis due to a unit electric charge per unit area of electrodes applied along i-axis (electrodes perpendicular to j-axis). For example g_{33} denotes field developed in direction 3 due to an applied stress in direction 3 when all other stresses are zero. It also denotes the strain developed in direction 3 due to a unit charge per unit area of electrodes applied along direction 3. In a similar way, g_{15} denotes shear strain induced around direction 2 due to a unit applied charge per unit electrode area with electrodes normal to direction l." [25]

Mathematically,

g = Field Developed/Applied Stress = Strain Developed/Applied Charge Density (6.22)

i.e.,

$$d_{31} = K\varepsilon_0 g_{31} \tag{6.23}$$

where, K is the relative dielectric constant of the material and ε_0 is the permittivity of free space.

6.5.2 Coupling Coefficient k_{ij}

"The coupling coefficient defines the ability of a piezoceramic material to transform electrical energy to mechanical energy or vice versa. This effect is employed in both the sensors (force, pressure, acceleration measurement) and actuators (efficiency) arena. Coupling squared shows the ratio of transformed energy and total energy input and the same coefficient is used for both conversions, electrical to mechanical and mechanical to electrical. For example, k_{31}^2 is the transformed electric energy causing mechanical strain in direction 1 with no external stress divided by electric energy input in direction 3. It is also the transformed mechanical energy causing electrical charge in direction 3 divided by the mechanical energy input as a result of stress in direction 1 with no other external stress." [25]

Mathematically,

k_{31}^2 = mechanical energy stored/electrical energy applied (6.24)

After detailed mathematical modeling, not a subject of current discussion, we arrive at the final equation,

$$k_{ij}^{\ 2} = \frac{d_{ij}^{\ 2}}{s_{ij}^{E} \varepsilon_{ij}^{T}} \tag{6.25}$$

where, $s_{ij}^{E} = \frac{1}{C^{E}}$, C^{E} being the short circuit stiffness.

These are the set of equations , correlating k_{31}, d_{31}, g_{31}, and the open circuit and short circuit stiffness for the piezoelectric materials. Solving these equations simultaneously for a consistent solution, one can now characterize any given piezoelectric material for its 31 constants. Given the scope and timeline of this work, exact characterization results at this stage have not been obtained but this still remains the starting point of future research. Laid out here is the general framework which is in

complete compliance with theory. Substituting actual values obtained in the previous chapters remains only an algebraic problem for the polymer fabric sensors developed at Clemson University.

Chapter 7

CONCLUSIONS AND FUTURE WORK

7.1 Conclusions:

As a part of this work, we have studied the process of Electrospinning in detail and optimized the process conditions for the fabrication of polymer based piezoelectric fabric with varying weight ratios of nanomaterials dispersed in the polymer matrix. A lookup table has been prepared for this purpose. The threshold of dispersion of nanomaterials has been validated experimentally against the noted theoretical thresholds.

In the next stage, the produced fabric sensors have been analyzed for their piezoelectric properties, in both frequency and time domain. Based on the initial frequency domain analysis, a macro level cantilever beam based test bench has been designed and validated experimentally to characterize piezoelectric materials. Conducting extensive experiments based on piezoelectric actuation, free initial condition induced vibrations and step and impulse responses, numerical data has been assembled for the characterization.

Following this experimental work, extensive numerical analysis in both simulink and MATLAB has been addressed to measure the piezoelectric constants. At this stage, coupling between the mechanical and electrical properties has been established and the concept of switch stiffness, introduced as a method for vibration suppression has been extended to model the coupling coefficient. Results have been verified using commercial piezo-actuators. Based on this modeling, a novel software switching function has been developed to implement the switch stiffness control law for vibration suppression in continuous systems. At this stage, the frequency domain analysis carried

out initially on the numerical data has been integrated into the derived mathematical model. As a result, the switch stiffness control law has been implemented in real time successfully.

Noting the delay of numerical analysis of data in the implementation of this control law to be significant, a novel approach of equivalent viscous damping has been introduced to develop an active vibration suppression method, implementing the switch stiffness control law by actuating the beam based on a voltage control signal designed from the equivalent viscous damping model. Finally, the methods of modal analysis and FEA have been compared as methods to obtain numerical solution to the EOM for vibrations in cantilever beams. Noting the deviation of solution from experimental measurement, a nonlinear strain based EOM has been derived and analyzed to give better results. The solution through FEA has been finally incorporated in the control as a feedforward control signal to obtain better vibration suppression characteristics.

Finally, a framework to completely characterize the piezoelectric materials for their 31 constants has been proposed based on a theory developed from the constitutive equations of piezoelectricity.

7.2 Scope for future work:

One of the primary objectives of this research still remains untouched. The existing control system based on image processing was to be updated with a nonlinear adaptive controller with both feedback and feedforward signals integrated into the structure. Given the unavailability of the right resources, this up gradation still remains to be analyzed. Furthermore, not all nanomaterials have been analyzed for enhancement in peizoeletric properties of the polymer fabric sensors. The scope of introducing boronitride SWNTs into polymer matrix of polymers like PVDF is large.

We have laid out the framework for complete characterization of piezoelectric materials with regards to their 31 properties but given the time, we have not been able to quantify the results. The proposed

framework has many applications and is generic for testing any new materials. The extension of the switch stiffness concept into an equivalent active vibration suppression method has opened up a large pool of applications where earlier the level of control voltage required was a big problem in using these materials. The exploration of these results in the area of NEMS and MEMS is probably the most important research in progress currently, i.e. the replacement of peizoresistive sensors with piezoelectric.

Appendix

A1: Source codes and supporting files for Chapter 4.

A1.1 Modal Analysis:

Main code:

```
close all;
clear all;
clc;

Eb=200e9;
Ep=15.857e9;
tb=0.254e-3;
tp=0.3e-3;
pb=8000;
pp=5887;
b=25.4e-3;
l=0.2794;
zn=Ep*tp*(tp+tb)/(2*(Eb*tb+Ep*tp));

x=0:0.0001:0.2794;

for i=1:1:length(x)
    if x(i)<0.01
        pA(i)=pb*b*tb;
        EI(i)=Eb*(tb^3)*b/12;
    elseif x(i)>=0.01&&x(i)<=0.05
        pA(i)=(pb*tb+pp*tp)*b;

EI(i)=(Eb*(tb^3)*b/12)+(Eb*tb*(zn^2)*b)+(Ep*b*(((tp^3)/3)+tp*(zn^2)+(tp*(tb/2
)^2+(tb/2)*(tp)^2)-zn*((tp)^2+tp*tb)));
    else
        pA(i)=pb*b*tb;
        EI(i)=Eb*(tb^3)*b/12;
    end
end

b1=1.875;
b2=4.694;
b3=7.855;
b4=11;

p1=pb*b*tb;
p2=(pb*tb+pp*tp)*b;

e1=Eb*(tb^3)*b/12;
```

```
e2=(Eb*(tb^3)*b/12)+(Eb*tb*(zn^2)*b)+(Ep*b*(((tp^3)/3)+tp*(zn^2)+(tp*(tb/2)^2
+(tb/2)*(tp)^2)-zn*((tp)^2+tp*tb)));

c1=0.2792434923;
c2=0.2764783324;
c3=0.2645214224;
c4=0.2454611406;

d1=0.0001099883709;
d2=0.002905396970;
d3=0.01490442909;
d4=0.03428048488;


for i=1:1:length(x)
    W1(i)=(1/sqrt(c1*p1+d1*p2))*(cos(b1*x(i)/l)-cosh(b1*x(i)/l)-
((cos(b1)+cosh(b1))/(sin(b1)+sinh(b1)))*(sin(b1*x(i)/l)-sinh(b1*x(i)/l)));
    W2(i)=(1/sqrt(c2*p1+d2*p2))*(cos(b2*x(i)/l)-cosh(b2*x(i)/l)-
((cos(b2)+cosh(b2))/(sin(b2)+sinh(b2)))*(sin(b2*x(i)/l)-sinh(b2*x(i)/l)));
    W3(i)=(1/sqrt(c3*p1+d3*p2))*(cos(b3*x(i)/l)-cosh(b3*x(i)/l)-
((cos(b3)+cosh(b3))/(sin(b3)+sinh(b3)))*(sin(b3*x(i)/l)-sinh(b3*x(i)/l)));
    W4(i)=(1/sqrt(c4*p1+d4*p2))*(cos(b4*x(i)/l)-cosh(b4*x(i)/l)-
((cos(b4)+cosh(b4))/(sin(b4)+sinh(b4)))*(sin(b4*x(i)/l)-sinh(b4*x(i)/l)));
end

g=9.81;

w1=(b1^2)*sqrt(e1/(p1*(l^4)));
w2=(b2^2)*sqrt(e1/(p1*(l^4)));
w3=(b3^2)*sqrt(e1/(p1*(l^4)));
w4=(b4^2)*sqrt(e1/(p1*(l^4)));

f1=(1/sqrt(c1*p1+d1*p2))*(-0.1746105568e-2);
f2=(1/sqrt(c2*p1+d2*p2))*(-0.9161232455e-2);
f3=(1/sqrt(c3*p1+d3*p2))*(-0.2124973153e-1);
f4=(1/sqrt(c4*p1+d4*p2))*(-0.3320559694e-1);

g1=(1/sqrt(c1*p1+d1*p2))*(-0.2170029190);
g2=(1/sqrt(c2*p1+d2*p2))*(-0.1120936582);
g3=(1/sqrt(c3*p1+d3*p2))*(-0.4985171868e-1);
g4=(1/sqrt(c4*p1+d4*p2))*(-0.1736926319e-1);

h1=(f1*p2+g1*p1)*g;
h2=(f2*p2+g2*p1)*g;
h3=(f3*p2+g3*p1)*g;
h4=(f4*p2+g4*p1)*g;

d31=-170e-12;

m1=-0.5*Ep*b*d31*(tb+tp-2*zn)*(1/sqrt(c1*p1+d1*p2))*(-2.2046);
m2=-0.5*Ep*b*d31*(tb+tp-2*zn)*(1/sqrt(c2*p1+d2*p2))*(-11.1321);
m3=-0.5*Ep*b*d31*(tb+tp-2*zn)*(1/sqrt(c3*p1+d3*p2))*(-11.9237);
m4=-0.5*Ep*b*d31*(tb+tp-2*zn)*(1/sqrt(c4*p1+d4*p2))*(9.3053);
```

```
x1=(1/sqrt(c1*p1+d1*p2))*(-0.4433564621e-1);
x2=(1/sqrt(c2*p1+d2*p2))*(-0.6748957114e-2);
x3=(1/sqrt(c3*p1+d3*p2))*(-0.1759136345e-2);
x4=(1/sqrt(c4*p1+d4*p2))*(-0.4194039318e-4);

y1=(1/sqrt(c1*p1+d1*p2))*(-0.6563514626e-4);
y2=(1/sqrt(c2*p1+d2*p2))*(-0.3400000479e-3);
y3=(1/sqrt(c3*p1+d3*p2))*(-0.7760827802e-3);
y4=(1/sqrt(c4*p1+d4*p2))*(-0.1185007279e-2);

c=-0.1;

ic1=c*(y1*p2+x1*p1);
ic2=c*(y2*p2+x2*p1);
ic3=c*(y3*p2+x3*p1);
ic4=c*(y4*p2+x4*p1);

ic=[ic1;0;ic2;0;ic3;0;ic4;0];

t=3;

v=1000;

omega=2*pi*6;

[t,response]=ode45('myfunc_q_sol',t,ic,[],w1,w2,w3,w4,m1,m2,m3,m4,h1,h2,h3,h4
,v,omega);

q1=response(:,1);
q2=response(:,3);
q3=response(:,5);
q4=response(:,7);

plot(t,q1)
hold on
plot(t,q2,'r')
plot(t,q3,'g')
plot(t,q4,'k')

A1=q1*W1;
A2=q2*W2;
A3=q3*W3;
A4=q4*W4;

A=A1+A2+A3+A4;

figure(2)

plot(t,A(:,2795))
```

Supplement file:

```
function
state_derivative=myfunc_q_sol(t,state,flag,w1,w2,w3,w4,m1,m2,m3,m4,h1,h2,h3,h
4,v,omega)

state_derivative=zeros(8,1);
state_derivative(1)=state(2);
state_derivative(3)=state(4);
state_derivative(5)=state(6);
state_derivative(7)=state(8);

state_derivative(2)=-(w1^2)*state(1)+m1*v*sin(omega*t)+h1;
state_derivative(4)=-(w2^2)*state(3)+m2*v*sin(omega*t)+h2;
state_derivative(6)=-(w3^2)*state(5)+m3*v*sin(omega*t)+h3;
state_derivative(8)=-(w4^2)*state(7)+m4*v*sin(omega*t)+h4;
```

A1.2 FEA of governing equation based on linear strain Euler Bernoulli Beam Theory:

Main Code:

```
close all;
clear all;
clc;

% Parameters
Eb=200e9;
Ep=15.857e9;
tb=0.254e-3;
tp=0.3e-3;
pb=8000;
pp=5887;
b=25.4e-3;
l=0.280;
zn=Ep*tp*(tp+tb)/(2*(Eb*tb+Ep*tp));

x=0:0.001:0.280;

for i=1:1:length(x)
    if x(i)<0.01
        pA(i)=pb*b*tb;
        EI(i)=Eb*(tb^3)*b/12;
    elseif x(i)>=0.01&&x(i)<=0.05
        pA(i)=(pb*tb+pp*tp)*b;

EI(i)=(Eb*(tb^3)*b/12)+(Eb*tb*(zn^2)*b)+(Ep*b*(((tp^3)/3)+tp*(zn^2)+(tp*(tb/2
)^2+(tb/2)*(tp)^2)-zn*((tp)^2+tp*tb)));
    else
        pA(i)=pb*b*tb;
        EI(i)=Eb*(tb^3)*b/12;
    end
end
```

```
% Constants Evaluation
he=x(2)-x(1);
M=(he/420)*[156,-22*he,54,13*he;-22*he,4*he^2,-13*he,-3*he^2;54,-
13*he,156,22*he;13*he,-3*he^2,22*he,4*he^2];
K1=(2/he^3)*[6,-3*he,-6,-3*he;-3*he,2*he^2,3*he,1*he^2;-6,3*he,6,3*he;-
3*he,1*he^2,3*he,2*he^2];
K2=(1/7)*[432/(5*he^5),-8/(he^2),-432/(5*he^5),-8/(he^2);-
18/(he^4),256/(15^he),18/(he^4),32/(15*he);-
432/(5*he^5),8/(he^2),432/(5*he^5),8/(he^2);-
18/(he^4),32/(15^he),18/(he^4),256/(15*he)];
num_node=length(x);
num_element=num_node-1;

K1_global=zeros(2*num_node,2*num_node);
K2_global=zeros(2*num_node,2*num_node);
M_global=zeros(2*num_node,2*num_node);

F=zeros(2*num_node,1);

% sid_elements=zeros(num_element,3);
% sid_nodes=zeros(num_node,2);
%
% for i=1:1:num_element
%     for j=1:1:3
%         if j==3
%             sid_elements(i,j)=i+1;
%         else
%             sid_elements(i,j)=i;
%         end
%     end
% end
% for i=1:1:num_node
%     for j=1:1:2
%         if j==1
%             sid_nodes(i,j)=i;
%         else
%             sid_nodes(i,j)=x(i);
%         end
%     end
% end

% Elemental Calculations and Assmbly
for i=1:1:num_element
    if x(i)==0.05
        k1=EI(i+1)*K1;
        k2=EI(i+1)*K2;
        m=pA(i+1)*M;
    else
        k1=EI(i)*K1;
        k2=EI(i)*K2;
        m=pA(i)*M;
    end
    for p=1:1:4
        for q=1:1:4
            K1_global(p+2*i-2,q+2*i-2)=K1_global(p+2*i-2,q+2*i-2)+k1(p,q);
```

```
            K2_global(p+2*i-2,q+2*i-2)=K2_global(p+2*i-2,q+2*i-2)+k2(p,q);
            M_global(p+2*i-2,q+2*i-2)=M_global(p+2*i-2,q+2*i-2)+m(p,q);
        end
    end
end

% Imposing BCs
K1_global_bc=zeros(2*num_node-2,2*num_node-2);
K2_global_bc=zeros(2*num_node-2,2*num_node-2);
M_global_bc=zeros(2*num_node-2,2*num_node-2);

for i=1:1:(2*num_node-2)
    for j=1:1:(2*num_node-2)
        K1_global_bc(i,j)=K1_global(i+2,j+2);
        K2_global_bc(i,j)=K2_global(i+2,j+2);
        M_global_bc(i,j)=M_global(i+2,j+2);
    end
end
% Minv=inv(M_global_bc);

% Time domain discretization

alpha=1/2;
gama=1/2;

t=0:0.01:1;

del_t=t(2)-t(1);

c1=gama*(del_t^2)/2;
c2=(1-gama)*(del_t^2)/2;
c3=(2*alpha)/(gama*del_t);
c4=((2*alpha)/(gama))-1;
c5=(((1*alpha)/(gama))-1)*del_t;

U=zeros((2*num_node-2),length(t));
U1=zeros((2*num_node-2),length(t));
U2=zeros((2*num_node-2),length(t));
A=zeros((2*num_node-2),length(t));
B=zeros((2*num_node-2),length(t));

for i=1:1:(2*num_node-2)
        if rem(i,2)==0
            U(i,1)=-(pi/(2*l))*sin((pi/(2*l))*x((i/2)+1));
        else
            U(i,1)=cos((pi/(2*l))*x(((i+1)/2)+1))-1;
        end
end
temp1=0;

for j=2:1:length(t)
    for k=1:1:100
        for q=1:1:(2*num_node-2)
```

```
            for r=1:1:(2*num_node-2)

A(q,j)=A(q,j)+(M_global_bc(q,r)+c1*K1_global_bc(q,r))*U(r,j)+c1*K2_global_bc(
q,r)*(U(r,j).^3)-M_global_bc(q,r)*(U(r,j-1)+del_t*U1(r,j-1)+c2*U2(r,j-1));
        if q==r

B(q,j)=B(q,j)+3*c1*K2_global_bc(q,r)*(U(r,j).^2)+(M_global_bc(q,r)+c1*K1_glob
al_bc(q,r));
        else

B(q,j)=B(q,j)+c1*K2_global_bc(q,r)*(U(r,j).^3)+(M_global_bc(q,r)+c1*K1_global
_bc(q,r))*U(r,j);
        end
            end
        end
        for i=1:1:(2*num_node-2)
        if abs(A(i,j))<0.00000000001
            temp1=1;
        else
            for p=1:1:(2*num_node-2)
                U(p,j)=U(p,j)-A(p,j)/B(p,j);
            end
            temp1=0;
            break
        end
        end
        for s=1:1:(2*num_node-2)
        U2(s,j)=(1/c1)*(U(s,j)-U(s,j-1))-(1/c1)*del_t*U1(s,j-1)-((1/gama)-
1)*U2(s,j-1);
        U1(s,j)=U1(s,j-1)+(1-alpha)*del_t*U2(s,j-1)+alpha*del_t*U2(s,j);
        end

        if temp1==1
            break
        end
%             k=k+1;



    end
%     for s=1:1:(2*num_node-2)
%           U2(s,j)=(1/c1)*(U(s,j)-U(s,j-1))-(1/c1)*del_t*U1(s,j-1)-((1/gama)-
1)*U2(s,j-1);
%         U1(s,j)=U1(s,j-1)+(1-alpha)*del_t*U2(s,j-1)+alpha*del_t*U2(s,j);
%     end
end
```

A1.3 FEA of governing equation based on nonlinear strain Euler Bernoulli Beam Theory:

Main code:

```
close all;
clear all;
```

```
clc;

% Parameters
Eb=200e9;
Ep=15.857e9;
tb=0.254e-3;
tp=0.3e-3;
pb=8000;
pp=5887;
b=25.4e-3;
l=0.280;
zn=Ep*tp*(tp+tb)/(2*(Eb*tb+Ep*tp));

x=0:0.001:0.280;

for i=1:1:length(x)
    if x(i)<0.01
        pA(i)=pb*b*tb;
        EI(i)=Eb*(tb^3)*b/12;
    elseif x(i)>=0.01&&x(i)<=0.05
        pA(i)=(pb*tb+pp*tp)*b;

EI(i)=(Eb*(tb^3)*b/12)+(Eb*tb*(zn^2)*b)+(Ep*b*(((tp^3)/3)+tp*(zn^2)+(tp*(tb/2
)^2+(tb/2)*(tp)^2)-zn*((tp)^2+tp*tb)));
    else
        pA(i)=pb*b*tb;
        EI(i)=Eb*(tb^3)*b/12;
    end
end
% Constants Evaluation
he=x(2)-x(1);
M=(he/420)*[156,-22*he,54,13*he;-22*he,4*he^2,-13*he,-3*he^2;54,-
13*he,156,22*he;13*he,-3*he^2,22*he,4*he^2];
K1=(2/he^3)*[6,-3*he,-6,-3*he;-3*he,2*he^2,3*he,1*he^2;-6,3*he,6,3*he;-
3*he,1*he^2,3*he,2*he^2];
K2=(1/7)*[432/(5*he^5),-8/(he^2),-432/(5*he^5),-8/(he^2);-
18/(he^4),256/(15^he),18/(he^4),32/(15*he);-432/(5*he^5),8/(he^2),...
    432/(5*he^5),8/(he^2);-18/(he^4),32/(15^he),18/(he^4),256/(15*he)];
K3=[-198/(35*he^4),-198/(35*he^4),-
198/(35*he^4),36/(35*he^3);36/(35*he^3),36/(35*he^3),-
6/(35*he^3),2/(7*he^2);...
    198/(35*he^4),198/(35*he^4),198/(35*he^4),-36/(35*he^3);-6/(35*he^3),-
6/(35*he^3),36/(35*he^3),-102/(35*he^2)];
K4=[648/(35*he^5),-4/(35*he^2),-648/(35*he^5),-4/(35*he^2);-
54/(35*he^4),6/(7*he),54/(35*he^4),2/(35*he);...
    -
648/(35*he^5),4/(35*he^2),648/(35*he^5),4/(35*he^2);54/(35*he^4),2/(35*he),54
/(35*he^4),6/(7*he)];
K5=[-198/(35*he^4),36/(35*he^3),198/(35*he^4),36/(35*he^3);-6/(35*he^3),-
102/(35*he^2),36/(35*he^3),-2/(7*he^2);...
    198/(35*he^4),-36/(35*he^3),198/(35*he^4),36/(35*he^3);-
36/(35*he^3),2/(7*he^2),-6/(35*he^3),102/(35*he^2)];
K6=[-72/(35*he^4),-36/(35*he^3),-
72/(35*he^4),36/(35*he^3);36/(35*he^3),18/(35*he^2),36/(35*he^3),-
18/(35*he^2);...
```

```
    72/(35*he^4),36/(35*he^3),72/(35*he^4),-
36/(35*he^3);36/(35*he^3),18/(35*he^2),36/(35*he^3),-18/(35*he^2)];
K7=[-648/(35*he^5),-4/(35*he^2),648/(35*he^5),-
4/(35*he^2);324/(35*he^4),2/(35*he),-324/(35*he^4),2/(35*he);...
    648/(35*he^5),4/(35*he^2),-
648/(35*he^5),4/(35*he^2);324/(35*he^4),2/(35*he),-324/(35*he^4),2/(35*he)];
K8=[-72/(35*he^4),36/(35*he^3),72/(35*he^4),-36/(35*he^3);36/(35*he^3),-
18/(35*he^2),36/(35*he^3),18/(35*he^2);...
    72/(35*he^4),-36/(35*he^3),72/(35*he^4),36/(35*he^3);36/(35*he^3),-
18/(35*he^2),36/(35*he^3),18/(35*he^2)];
K9=[108/(7*he^4),-12/(7*he^3),108/(7*he^4),12/(7*he^3);-
144/(35*he^3),16/(35*he^2),-12/(7*he^3),-16/(35*he^2);...
    -108/(7*he^4),12/(7*he^3),-108/(7*he^4),-12/(7*he^3);-
12/(7*he^3),16/(35*he^2),-144/(35*he^3),-16/(35*he^2)];



num_node=length(x);
num_element=num_node-1;

K1_global=zeros(2*num_node,2*num_node);
K2_global=zeros(2*num_node,2*num_node);
K3_global=zeros(2*num_node,2*num_node);
K4_global=zeros(2*num_node,2*num_node);
K5_global=zeros(2*num_node,2*num_node);
K6_global=zeros(2*num_node,2*num_node);
M_global=zeros(2*num_node,2*num_node);

% Time domain discretization

alpha=1/2;
gama=1/2;

t=0:0.001:1;

del_t=t(2)-t(1);

c1=gama*(del_t^2)/2;
c2=(1-gama)*(del_t^2)/2;
c3=(2*alpha)/(gama*del_t);
c4=((2*alpha)/(gama))-1;
c5=(((1*alpha)/(gama))-1)*del_t;

U=zeros((2*num_node),length(t));
U1=zeros((2*num_node),length(t));
U2=zeros((2*num_node),length(t));
A=zeros((2*num_node),length(t));
B=zeros((2*num_node),length(t));

for i=1:1:(2*num_node)
        if rem(i,2)==0
            U(i,1)=-(pi/(2*l))*sin((pi/(2*l))*x((i/2)));
        else
```

```
            U(i,1)=cos((pi/(2*l))*x(((i+1)/2)))-1;
        end
end
temp1=0;


for j=2:1:length(t)
for i=1:1:(num_element)
    if x(i)==0.05
        k1=EI(i+1)*K1;
        k2=EI(i+1)*K2;
        k3=EI(i+1)*K3;
        k4=EI(i+1)*K4;
        k5=EI(i+1)*K5;
        k6=EI(i+1)*K6;
        k7=EI(i+1)*K7;
        k8=EI(i+1)*K8;
        k9=EI(i+1)*K9;
        m=pA(i+1)*M;
    else
        k1=EI(i)*K1;
        k2=EI(i)*K2;
        k3=EI(i)*K3;
        k4=EI(i)*K4;
        k5=EI(i)*K5;
        k6=EI(i)*K6;
        k7=EI(i)*K7;
        k8=EI(i)*K8;
        k9=EI(i)*K9;
        m=pA(i)*M;
    end
    for p=1:1:4
        for q=1:1:4
            K1_global(p+2*i-2,q+2*i-2)=K1_global(p+2*i-2,q+2*i-2)+k1(p,q);
            K2_global(p+2*i-2,q+2*i-2)=K2_global(p+2*i-2,q+2*i-2)+k2(p,q);
            if q==1
                  K3_global(p+2*i-2,q+2*i-2)=K3_global(p+2*i-2,q+2*i-
2)+(k3(p,q)+k6(p,q))*U(1+2*i-2+1,j-1);
            elseif q==2
                  K3_global(p+2*i-2,q+2*i-2)=K3_global(p+2*i-2,q+2*i-
2)+(k3(p,q)+k6(p,q))*U(1+2*i-2+2,j-1);
            elseif q==3
                  K3_global(p+2*i-2,q+2*i-2)=K3_global(p+2*i-2,q+2*i-
2)+(k3(p,q)+k6(p,q))*U(1+2*i-2+3,j-1);
            else
                  K3_global(p+2*i-2,q+2*i-2)=K3_global(p+2*i-2,q+2*i-
2)+(k3(p,q)+k6(p,q))*U(1+2*i-2,j-1);
            end
            if q==1
                  K4_global(p+2*i-2,q+2*i-2)=K4_global(p+2*i-2,q+2*i-
2)+(k4(p,q)+k7(p,q))*U(1+2*i-2+2,j-1);
            elseif q==2
                  K4_global(p+2*i-2,q+2*i-2)=K4_global(p+2*i-2,q+2*i-
2)+(k4(p,q)+k7(p,q))*U(1+2*i-2+3,j-1);
            elseif q==3
```

```
                K4_global(p+2*i-2,q+2*i-2)=K4_global(p+2*i-2,q+2*i-
2)+(k4(p,q)+k7(p,q))*U(1+2*i-2,j-1);
            else
                K4_global(p+2*i-2,q+2*i-2)=K4_global(p+2*i-2,q+2*i-
2)+(k4(p,q)+k7(p,q))*U(1+2*i-2+1,j-1);
            end
            if q==1
                K5_global(p+2*i-2,q+2*i-2)=K5_global(p+2*i-2,q+2*i-
2)+(k5(p,q)+k8(p,q))*U(1+2*i-2+3,j-1);
            elseif q==2
                K5_global(p+2*i-2,q+2*i-2)=K5_global(p+2*i-2,q+2*i-
2)+(k5(p,q)+k8(p,q))*U(1+2*i-2,j-1);
            elseif q==3
                K5_global(p+2*i-2,q+2*i-2)=K5_global(p+2*i-2,q+2*i-
2)+(k5(p,q)+k8(p,q))*U(1+2*i-2+1,j-1);
            else
                K5_global(p+2*i-2,q+2*i-2)=K5_global(p+2*i-2,q+2*i-
2)+(k5(p,q)+k8(p,q))*U(1+2*i-2+2,j-1);
            end
            if q==1
                K6_global(p+2*i-2,q+2*i-2)=K6_global(p+2*i-2,q+2*i-
2)+(k9(p,q))*U(1+2*i-2+1,j-1)*U(1+2*i-2+2,j-1);
            elseif q==2
                K6_global(p+2*i-2,q+2*i-2)=K6_global(p+2*i-2,q+2*i-
2)+(k9(p,q))*U(1+2*i-2+2,j-1)*U(1+2*i-2+3,j-1);
            elseif q==3
                K6_global(p+2*i-2,q+2*i-2)=K6_global(p+2*i-2,q+2*i-
2)+(k9(p,q))*U(1+2*i-2+3,j-1)*U(1+2*i-2,j-1);
            else
                K6_global(p+2*i-2,q+2*i-2)=K6_global(p+2*i-2,q+2*i-
2)+(k9(p,q))*U(1+2*i-2,j-1)*U(1+2*i-2+1,j-1);
            end
            M_global(p+2*i-2,q+2*i-2)=M_global(p+2*i-2,q+2*i-2)+m(p,q);
        end
    end

    for k=1:1:100
        for pq=1:1:(2*num_node)
            for r=1:1:(2*num_node)

A(pq,j)=A(pq,j)+(M_global(pq,r)+c1*(K1_global(pq,r)+K6_global(pq,r)))*U(r,j)+
c1*K2_global(pq,r)*(U(r,j).^3)+c1*(K3_global(pq,r)+K4_global(pq,r)+K5_global(
pq,r))*(U(r,j).^2)-M_global(pq,r)*(U(r,j-1)+del_t*U1(r,j-1)+c2*U2(r,j-1));
        if pq==r

B(pq,j)=B(pq,j)+3*c1*K2_global(pq,r)*(U(r,j).^2)+(M_global(pq,r)+c1*(K1_globa
l(pq,r)+K6_global(pq,r)))+2*c1*(K3_global(pq,r)+K4_global(pq,r)+K5_global(pq,
r))*(U(r,j));
        else

B(pq,j)=B(pq,j)+c1*K2_global(pq,r)*(U(r,j).^3)+(M_global(pq,r)+c1*(K1_global(
pq,r)+K6_global(pq,r)))*U(r,j)+c1*(K3_global(pq,r)+K4_global(pq,r)+K5_global(
pq,r))*(U(r,j).^2);
        end
            end
```

```
        end
        for n=3:1:(2*num_node)
        if abs(A(n,j))<0.00000000001
            temp1=1;
        else
            for mn=3:1:(2*num_node)
                U(mn,j)=U(mn,j)-A(mn,j)/B(mn,j);
            end
            U(1,j)=0;
            U(2,j)=0;
            temp1=0;
            break
        end
        end
        for s=1:1:(2*num_node)
        U2(s,j)=(1/c1)*(U(s,j)-U(s,j-1))-(1/c1)*del_t*U1(s,j-1)-((1/gama)-
1)*U2(s,j-1);
        U1(s,j)=U1(s,j-1)+(1-alpha)*del_t*U2(s,j-1)+alpha*del_t*U2(s,j);
        end

        if temp1==1
            break
        end
%             k=k+1;


    end
%     for s=1:1:(2*num_node-2)
%           U2(s,j)=(1/c1)*(U(s,j)-U(s,j-1))-(1/c1)*del_t*U1(s,j-1)-((1/gama)-
1)*U2(s,j-1);
%         U1(s,j)=U1(s,j-1)+(1-alpha)*del_t*U2(s,j-1)+alpha*del_t*U2(s,j);
%     end
end
end
```

REFERENCES

[1] http://en.wikipedia.org/wiki/Piezoelectricity, Accessed May 2009

[2] http://en.wikipedia.org/wiki/Nanotechnology, Accessed May 2009

[3] http://en.wikipedia.org/wiki/Electrospinning, Accessed May 2009

[4] http://en.wikipedia.org/wiki/Spin_coating, Accessed May 2009

[5] http://www.ntcresearch.org/pdf-rpts/AnRp07/M04-CL05-A7.pdf

[6] Mohsen Dadfarnia, Lyapunov-Based Piezoelectric. Control of Hybrid Flexible Structures, Chapters 2 and 3, August 2003.

[7] Arun Ramaratnam and Dr. Nader Jalili, "A switched stiffness approach for structural vibration control: theory and real-time implementation", *Journal of Sound and Vibration*, 291, pp. 258-274, August 2005.

[8] W. W. Clark, "Vibration Control with State-Switched Piezoelectric Materials", *Journal of Intelligent Material Systems and Structures*, 11, pp. 263-271, 2000.

[9] Inbook, Rao S. S., ed., 2007. Vibration of Continuous Media, John Wiley & Sons, Inc., Hoboken, NJ, Chap. 11, pp.322-325.

[10] Bao-Zhu Guo, Jun-Min Wang and Kun-Yi Yang, "Dynamic stabilization of an Euler–Bernoulli beam under boundary control and non-collocated observation", *Systems and Control Letters*, 57, pp. 740-749, 2008.

[11] Ricardo Guerra, Claudiu Iurian and Leonardo Acho, "Velocity Observer for Mechanical Systems", New Developments in Robotics, Automation and Control, pp. 111-120.

[12] M. Dadfarnia, N. Jalili, B. Xian and D. M. Dawson, "Lyapunov-Based Vibration Control of Translational Euler-Bernoulli Beams Using the Stabilizing Effect of Beam Damping Mechanisms", *Journal of Vibration and Control*, 10, pp. 933, 2004.

[13] Banks, H. T. and Inman, D. J., "On damping mechanisms in beams", *Transactions of the ASME, Journal of Applied* Mechanics, **58 (3)**, 716–723, 1991.

[14] Dadfarnia M., Jalili, N., Liu, Z., and Dawson, D. M., "An observer-based piezoelectric control of flexible Cartesian robot manipulators: theory and experiment", *Journal of Control Engineering Practice,* in press 1–13, 2004.

[15] de Querioz, M. S., Dawson, D. M., Nagarkatti, S. P. and Zhang, F., "Lyapunov-Based Control of Mechanical Systems", Birkhauser, Boston, 2000.

[16] M. Dadfarnia, N. Jalili, B. Xian, D.M. Dawson, "A Lyapunov-based piezoelectric controller for flexible Cartesian robot manipulators", *ASME Journal of Dynamic Systems, Measurements and Control*, 126 (2), pp. 347–358, 2004.

[17] N.W. Hagood, A. Von Flotow, "Damping of structural vibrations with piezoelectric materials and passive electrical networks", *Journal of Sound and Vibration*, 146 (2), pp. 243–268, 1991.

[18] N. Jalili, "A new perspective for semi-automated structural vibration control", *Journal of Sound and Vibration*, 238 (3), pp. 481–494, 2000.

[19] N. Jalili, "A comparative study and analysis of semi-active vibration-control systems", *ASME Journal of Vibration and Acoustics,* 124, pp. 593–605, 2002.

[20] A. Ramaratnam, N. Jalili, M. Grier, "Piezoelectric vibration suppression of translational flexible beams using switched stiffness", Proceedings of 2003 International Mechanical Engineering Congress and Exposition (IMECE 2003-41217), Washington DC, 2003.

[21] A. Ramaratnam, Semi-active vibration control using piezoelectric-based switched stiffness, Master's Thesis, Department of Mechanical Engineering, Clemson University, 2004.

[22] B. Xian, M.S. de Queiroz, D.M. Dawson, M.L. McIntyre, "Output feedback variable structure control of nonlinear mechanical systems", Proceedings of IEEE Conference on Decision and Control, Hawaii, 2003.

[23] M.A. Franchek, M.W. Ryan, R.J. Bernhard, "Adaptive passive vibration control", *Journal of Sound and Vibration* 189 (5), pp. 565–585, 1995.

[24] Inbook, Reddy J. N., 2005, ed. 3, An Introduction to the Finite Element Method (Engineering Series), Beam elements and frame elements.

[25] Dr. Jalili, Notes: ME 893, Spring 2008.